Failure probability estimation through high-dimensional elliptical distribution modeling with multiple importance sampling

Marie Chiron, Christian Genest, Jérôme Morio, Sylvain Dubreuil

Reliability Engineering and System Safety 235 (2023) 109238

Contents lists available at ScienceDirect

Reliability Engineering and System Safety

journal homepage: www.elsevier.com/locate/ress

Failure probability estimation through high-dimensional elliptical distribution modeling with multiple importance sampling

Marie Chiron [a,*], Christian Genest [b], Jérôme Morio [a], Sylvain Dubreuil [a]

[a] ONERA/DTIS, Université de Toulouse, F-31055 Toulouse, France
[b] Department of Mathematics and Statistics, McGill University, Montréal (Québec), Canada

ARTICLE INFO

Keywords:
Elliptical distribution
High dimension
Multiple importance sampling
Reliability analysis
Simulation method

ABSTRACT

This paper addresses the challenge of performing importance sampling in high-dimensional space (several hundred inputs) in order to estimate the failure probability of a physical system subject to randomness. It is assumed that the failure domain defined in the input space can possibly include multiple failure regions. A new approach is developed to construct auxiliary importance sampling densities sequentially for each failure region identified as part of the failure domain. The search for failure regions is achieved through optimization. A stochastic decomposition of the elliptically distributed inputs is exploited in the structure of the auxiliary densities, which are expressed as the product of a parametric conditional distribution for the radial component, and a parametric von Mises–Fisher distribution for the directional vector. The failure probability is then estimated by multiple importance sampling with a mixture of the densities. To demonstrate the efficiency of the proposed method in high-dimensional space, several numerical examples are considered involving the multivariate Gaussian and Student distributions, which are commonly used elliptical distributions for input modeling. In comparison with other simulation methods, the numerical cost of the proposed approach is found to be quite low when the gradient of the performance function defining the failure domain is available.

1. Introduction

Estimation of the failure probability of an engineering system is a major challenge in reliability analysis, especially when a large number of input variables is involved. Suppose that subject to a location shift, the unknown values of these variables can be represented by a d-variate continuous uncorrelated random vector $\mathbf{X}$ with zero mean, where $d \geq 50$, say. Further assume that the vector $\mathbf{X}$ is elliptically distributed [1–3], which is the case for the Gaussian and Student distributions, among others. The vector $\mathbf{X}$ can then be expressed in the form $\mathbf{X} = R\,\mathbf{T}$ in terms of a positive random variable R with fixed distribution and a d-variate random vector $\mathbf{T}$ which is independent of R and uniformly distributed on the unit sphere $\mathcal{T}_d = \{(t_1, \ldots, t_d) \in \mathbb{R}^d : t_1^2 + \cdots + t_d^2 = 1\}$.

The engineering system is modeled with a black-box function M which depends on $\mathbf{X}$ and is assumed to be numerically expensive. The failure domain D_f is defined as the set of outcomes $M(\mathbf{X}) = M(R\mathbf{T})$ for which a performance function g takes non-positive values, viz. $D_f = \{r\mathbf{t} : g[M(r\mathbf{t})] \leq 0\}$. For simplicity, the function $g \circ M$ will be written g and referred to as the *limit state function* (lsf).

This paper focuses on failure probability estimation with failure domains D_f comprising possibly several failure modes [4]. The failure is supposed to be a rare event and its probability is defined by the integral

$$P_f = \int_{D_f} f_R(r) f_{\mathbf{T}}(\mathbf{t})\,\mathrm{d}r\mathrm{d}\mathbf{t} = \int_{\mathbb{R}_+}\int_{\mathcal{T}_d} \mathbb{I}_{D_f}(r\mathbf{t}) f_R(r) f_{\mathbf{T}}(\mathbf{t})\,\mathrm{d}r\mathrm{d}\mathbf{t} = \mathbb{E}_{f_R, f_{\mathbf{T}}}\left[\mathbb{I}_{D_f}(R\mathbf{T})\right], \quad (1)$$

where f_R is the probability density function (pdf) of the random variable R and $f_{\mathbf{T}}$ is the joint pdf of the random vector $\mathbf{T}$. The indicator function $\mathbb{I}_{D_f}(r\mathbf{t})$ is equal to 1 if $g(r\mathbf{t}) \leq 0$ and 0 otherwise. The operator $\mathbb{E}_{f_R, f_{\mathbf{T}}}$ stands for mathematical expectation with respect to R and $\mathbf{T}$ simultaneously.

It is often impossible to evaluate the integral given by Eq. (1) analytically. Therefore, several approaches have been proposed to estimate Eq. (1) accurately with as few evaluations of g as possible; they typically involve approximation methods, simulation techniques [5] or both [6,7]. In low-dimensional input space, approximation techniques such as the first- and second-order reliability method (FORM/SORM) for multiple design points [8] and the surrogate-assisted method [9] are efficient. In the FORM/SORM method, the lsf is approximated with a Taylor expansion around the so-called design points, while in the

* Corresponding author.
E-mail address: marie.chiron@onera.fr (M. Chiron).

https://doi.org/10.1016/j.ress.2023.109238
Received 19 August 2022; Received in revised form 17 January 2023; Accepted 9 March 2023
Available online 13 March 2023

List of Abbreviations

CE-AIS	Cross-entropy based adaptive importance sampling
CV	Coefficient of variation
DS	Directional sampling
FORM/SORM	First- and second-order reliability method
iCE-vMFNM	Improved cross-entropy von Mises–Fisher–Nakagami mixture
iid	independent and identically distributed
IS	Importance sampling
KL	Kullback–Leibler
LB	Lower bound
LHS	Latin hypercube sampling
LS	Line sampling
lsf	limit state function
MBIS	Multisphere-based importance sampling
MC	Monte Carlo
MCMC	Markov chain Monte Carlo
MIS	Multiple importance sampling
MLE	Maximum likelihood estimation
pdf	probability density function
RBIS	Radial-based importance sampling
SS	Subset simulation
UB	Upper bound
VM	Variance minimization
vMF	von Mises–Fisher

surrogate-assisted method the lsf is approximated with a surrogate model constructed from training points [10,11]. Numerically inexpensive approximations of the lsf are then obtained. However, these techniques generally do not perform well in high-dimensional input spaces, as their performance deteriorates with increased dimension and their accuracy is jeopardized. Therefore, several approaches have been recently developed in order to solve this problem by mapping the high-dimensional inputs into a lower dimensional space [7], using the subset active subspace method [12] or a sufficient dimension reduction method [13] for instance. The limit state function metamodel is then built in the lower dimensional space.

Simulation methods are based on the crude Monte Carlo (MC) method [14] which is robust, irrespective of the dimension d and the complexity of g. After generating a sample of inputs of size N, the probability is estimated by the sample mean of the failure domain indicator function. However, the MC method is very costly in terms of evaluation of the lsf because its variance, given by $P_f(1-P_f)/N$, decreases slowly with N. To reduce the variance of the MC estimate and improve convergence, advanced simulation techniques can be used, such as subset simulation (SS) [15,16], importance sampling (IS) [17,18], line sampling (LS) [19,20] and directional sampling (DS) [21,22].

The focus of this paper is on importance sampling. The main idea of IS is to introduce an auxiliary density h whose support includes the support of $\mathbb{I}_{D_f} f_R f_{\mathbf{T}}$ in the integral (1), viz.

$$P_f = \int_{\mathbb{R}_+}\int_{\mathcal{T}_d} \mathbb{I}_{D_f}(r\mathbf{t})\,\frac{f_R(r)f_{\mathbf{T}}(\mathbf{t})}{h(r,\mathbf{t})}\,h(r,\mathbf{t})\,\mathrm{d}r\mathrm{d}\mathbf{t} = \mathbb{E}_h\left[\mathbb{I}_{D_f}(R\mathbf{T})\,\frac{f_R(R)f_{\mathbf{T}}(\mathbf{T})}{h(R,\mathbf{T})}\right].$$

The IS estimate of P_f and its coefficient of variation (CV) are then respectively given by

$$\hat{P}_f^{\mathrm{IS}} = \frac{1}{N}\sum_{i=1}^{N} \mathbb{I}_{D_f}(R_i\mathbf{T}_i)\,\frac{f_R(R_i)f_{\mathbf{T}}(\mathbf{T}_i)}{h(R_i,\mathbf{T}_i)} \quad \text{and} \quad \mathrm{CV} = \sqrt{\mathrm{var}(\hat{P}_f^{\mathrm{IS}})}/\hat{P}_f^{\mathrm{IS}}, \tag{2}$$

where the random pairs $(R_1,\mathbf{T}_1),\dots,(R_N,\mathbf{T}_N)$ are mutually independent and identically distributed (iid) with density h. The efficiency of the auxiliary density h depends on its ability to generate more observations in the failure domain than $f_R f_{\mathbf{T}}$. The variance, and hence also the CV, of the IS estimate can then be drastically reduced compared to those of the crude MC. The theoretically optimal IS density, which leads to a zero variance IS probability estimate, is given by

$$h_{\mathrm{opt}}(r,\mathbf{t}) = \mathbb{I}_{D_f}(r\mathbf{t})f_R(r)f_{\mathbf{T}}(\mathbf{t})/P_f. \tag{3}$$

However, this density h_{opt} is unavailable in practice as it depends on the quantity of interest, P_f. The goal of IS methods is then to construct an auxiliary density which is as close as possible to the optimal one, so that the greatest possible variance reduction can be achieved.

In low-dimensional space (say $d \leq 50$), IS methods for inputs that can be decomposed in the form $R\,\mathbf{T}$ have already been considered in the special case of the standard Gaussian distribution. The radial-based importance sampling method (RBIS) studied in [23,24] improved the numerical performance of the IS method by narrowing down the search to (typically large) values of the radial component associated with the failure domain. This approach inspired many developments, notably the recent multisphere-based importance sampling method (MBIS) in [25]. Studies on the directional component have also been conducted, e.g., in [26], where DS is performed on direction vectors generated from a mixture of von Mises–Fisher (vMF) distributions [27]. The number of components in the mixture, which corresponds to the number of failure modes, is selected by a clustering approach (DBSCAN algorithm used in [28]) but the procedure performs poorly in large dimension [29].

In high-dimensional input space, the radial component of the elliptical variable, representing its Euclidean norm, has higher value. For instance, the mean value of the radial component of a standard Gaussian variable is near $\sqrt{d}$ with a variance converging to $1/2$; see [30]. An important ring is then defined with two hyperspheres of radius LB and UB (for lower bound and upper bound, respectively) so that the interval $[\mathrm{LB},\mathrm{UB}]$ encompasses most of the probability mass of the radial component. Taking into account the important ring of standard Gaussian variables, the method proposed in [31] focuses on finding an optimal IS radial distribution within this important interval $[\mathrm{LB},\mathrm{UB}]$, without modifying $f_{\mathbf{T}}$. In contrast, the method proposed in [32] sets R as a deterministic variable equal to $\sqrt{d}$ and focuses on finding an optimal IS density for the vector $\mathbf{T}$ using a vMF mixture distribution. The latter method is generalized in [33] by combining it with an optimal parametric model for the radial distribution. However, the number of failure modes remains difficult to estimate in the absence of information concerning the failure domain.

The method proposed herein follows the work of [32,33] as it retains the idea of creating a mixture of densities to take into account the multiple failure modes. More precisely, the densities are assembled as a product of a density for the radial component, R, and another for the directional component, $\mathbf{T}$. However, the composition of the final IS density mixture differs from the previous methods in that it is built gradually as the different failure regions are being found.

The search for the failure regions is accomplished with the identification, through optimization, of the failing points closest to the origin in the standard elliptical space. These optimization procedures are inspired by the FORM/SORM methods in the case of multiple design points, but an original adaptation of the optimization is proposed in order to take into account the important ring. It is assumed that the gradient of the lsf is known, as in [34], for this optimization problem.

For each identified failure region, a single IS density is constructed as a product of a conditional density on R, as in the RBIS method, and a vMF density for the vector $\mathbf{T}$. For each failure region, the set of density parameters is derived and an optimization is performed with a Cross-Entropy based Adaptive IS algorithm (CE-AIS); see [35,36]. This new way of constructing the final IS density mixture proves to be simpler and requires fewer evaluations of the lsf. Moreover, the proposed failure probability estimate takes advantage of the multiple importance sampling (MIS) framework to reuse all the generated samples [7,18].

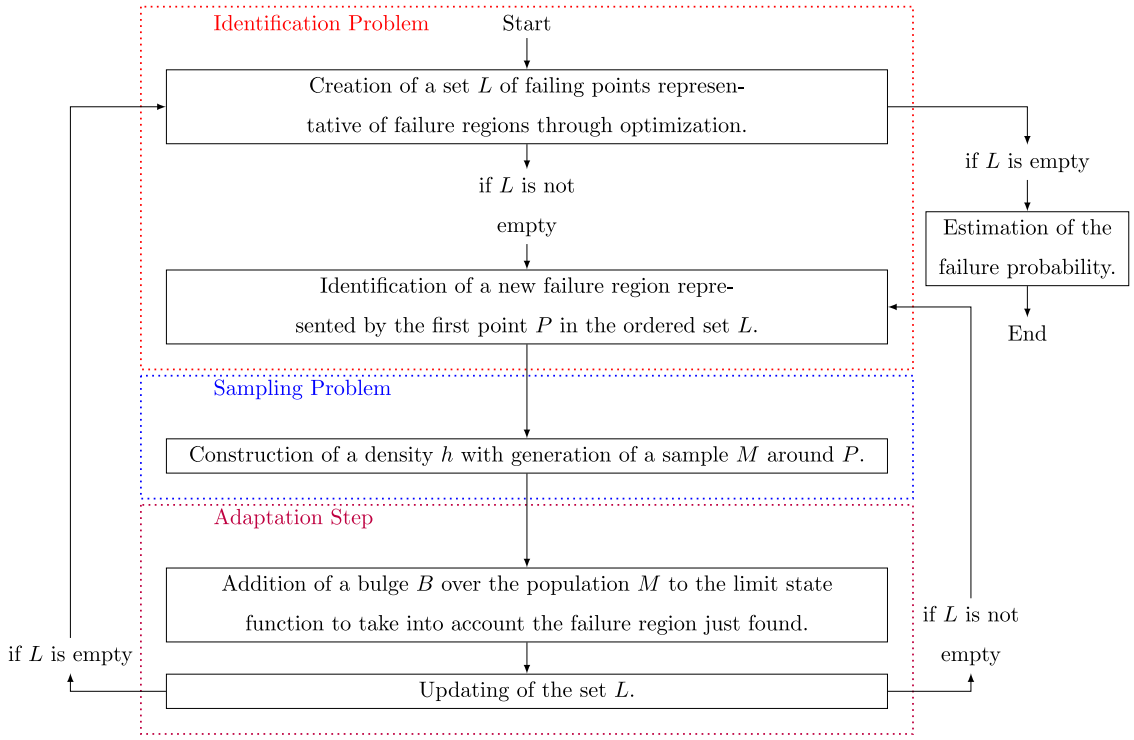

Fig. 1. Scheme of the proposed method to find and model every failure region.

This paper adds to the previous literature on the subject in being the first to use multiple importance sampling in high-dimensional space for elliptical distributions; to generalize auxiliary distributions based on a stochastic decomposition of the inputs for other elliptical distributions than the Gaussian distribution; and to use an adaptive search for the multiple failure regions of the failure domain. A complete description of the proposed algorithm is detailed in Section 2. Four numerical examples with elliptical inputs illustrate the performance of the proposed method in Section 3: three with the Gaussian distribution and one with the Student distribution. The results are summarized and some conclusions are drawn in Section 4.

2. High-dimensional failure probability estimation with multiple importance sampling

It is taken for granted that the limit state function (lsf) is complex, and hence that several failure regions in the high-dimensional input space have to be identified in order to get an accurate estimate of the failure probability. Instead of trying to sample in the failure domain as a whole with a mixture of densities optimized together as done in [32,33], the method proposed here sequentially identifies and generates samples in each of the failure regions. The final failure probability estimate is then computed with a mixture of the optimized single IS auxiliary densities.

2.1. Presentation of the proposed method and MIS estimate

In order to estimate the failure probability, it is proposed to decompose the problem in two parts. First, an identification problem is considered which consists of identifying the different regions of the failure domain in the input space. Next, a sampling problem is solved by constructing an optimized auxiliary density for each failure region. Although these two problems are distinct, they are intertwined and cannot be solved separately. As soon as a failure region is found, the construction of its IS auxiliary density is considered. Next, the search for a new failure region is initiated, taking into account the failure region previously found; this is the adaptation step. This scheme is repeated until all failure regions have been found and sampled as illustrated in Fig. 1.

Section 2.2 details the search for a set L of failing points which are representative of the failure regions, and the selection of a first failure region to be sampled. The sampling problem for this failure region is then considered in Section 2.3. The adaptation step in described in Section 2.4, as well as the loop which must be initiated when the set L is not empty after the adaptation step. The procedure to be followed when the set L is empty after the adaptation step is laid out in Section 2.5.

At the end of this scheme, every failure region has been identified and sampled, and the failure probability can be estimated by the MIS method [18]. For every failure region j, a number $n_j + 1$ of densities $h_{j,0}, \dots, h_{j,n_j}$ are created successively in the construction of the optimal density for the sampling problem derived in Section 2.3. They result from the parameter optimization process with $h_{j,0}$ being the initial density and h_{j,n_j} the optimized density that best fits the failure region. Instead of using only the last density h_{j,n_j} and its sample to represent the failure region j, all intermediate densities and samples are included to improve the stability of the estimate.

Let K denote the number of failure regions. Then the MIS probability estimate is given by

$$\hat{P}_f^{\mathrm{MIS}} = \frac{1}{N_{\mathrm{samp}}} \sum_{i=1}^{N_{\mathrm{samp}}} \mathbb{I}_{D_f}(R_i \mathbf{T}_i) \frac{f_R(R_i) f_{\mathbf{T}}(\mathbf{T}_i)}{h_{\mathrm{MIS}}(R_i \mathbf{T}_i)}, \quad R_i \mathbf{T}_i \sim h_{\mathrm{MIS}}$$

with

$$h_{\mathrm{MIS}}(r\mathbf{t}) = \frac{1}{n_{\mathrm{total}}} \sum_{j=1}^{K} \sum_{\ell=0}^{n_j} h_{j,\ell}(r, \mathbf{t}),$$

where the random pairs $(R_1, \mathbf{T}_1), (R_2, \mathbf{T}_2), \dots$ are iid conditionally on the parameter values which may be estimates. In the latter case, the random pairs are conceivably dependent on the information used to derive these estimates, but such dependence can be safely assumed to be negligible. Here, N_{samp} is the total number of observations generated in the various sampling problems performed for the estimation of the

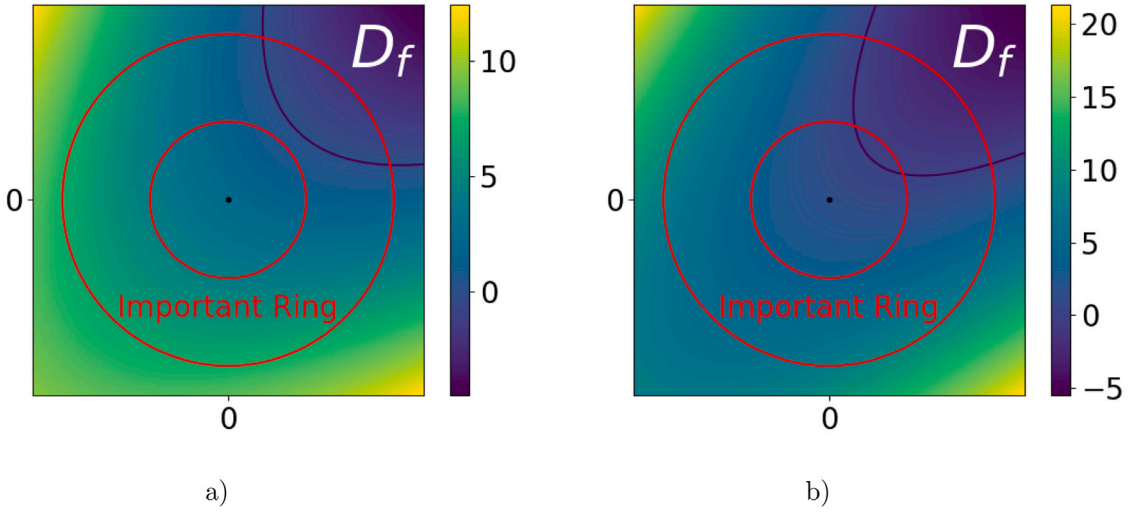

Fig. 2. Illustration of the location of the failure region and the important ring in (a) Case 1 where the closest failing point of the failure region is inside the important ring, and in (b) Case 2 where the closest failing point of the failure region is outside the important ring. The red circles delineate the lower bound and the upper bound of the important ring. In both examples, there is only one failure region in the failure domain, located in the upper right corner delimited in black.

failure probability, and the total number of densities in the mixture is n_{total}. The number n_{total} of IS auxiliary densities is equal to $n_1 + \cdots + n_K + K$. The following sections describe the successive steps of the method summarized in Fig. 1 to determine a valuable IS mixture density h_{MIS}.

2.2. Identification problem: Search for the failure regions through optimization

The search for the failure regions is inspired by what is achieved in the approximation methods FORM/SORM for multiple design points. In those methods, each failure region is identified with the failing point closest to the origin in the standard elliptical space [8,37]. Indeed the closest failing point, the so-called design point or most probable point [24], of a failure region is the most likely single realization of the input random variables that causes failure. Nevertheless, as reported in [30], in high-dimensional standard normal space those design points seldom belong to the important ring. Hence they are of little interest in the search for the main failure regions in such a space, as the probability mass associated with their surrounding space is negligible. To take this issue into account, the solution proposed here is to look for the closest failing points inside the important ring.

For each failure region, depending on its location with respect to the important ring, two different situations must be considered. In Case 1, the closest failing point of the failure region is inside the important ring. In Case 2, the closest failing point of the failure region does not belong to the important ring, as it is closer than the lower bound LB of the important interval, and the failure region spreads across the important ring. Case 2 is typical of contexts where the distribution of the radial component R leads to a particularly narrow important ring.

Fig. 2 provides schematic illustrations of the two cases. In each one of these situations, the failure region is identified with a failing point found as follows:

Case 1: The failure region is identified with the closest failing point. The local optimization problem is written in the form

$$P^* = \underset{\mathbf{x} \in \text{Imp.Ring} \cap D_f}{\operatorname{argmin}} \|\mathbf{x}\|, \tag{4}$$

where P^* is a point belonging to both the failure domain D_f and the important ring (Imp.Ring), which minimizes the Euclidean norm $\|\cdot\|$; see Fig. 3 (a). It is assumed that the gradient ∇g of the limit state function g is available, so that a gradient algorithm can be used to perform the optimization.

Case 2: The failure region is identified with a failing point resulting from two optimizations, as optimization (4) then has an infinite number of solutions: any point in the failure region on the lower bound LB of the important ring is a solution to problem (4). It is assumed that the optimizer then randomly selects one of them, say P^*. A second optimization is performed to find a point that would better represent this particular failure region. The proposed solution consists of finding the point $\tilde{P}^*$ that minimizes the limit state function in the lower bound LB of the important ring, viz.

$$\tilde{P}^* = \underset{\mathbf{x} \in \text{LB} \cap D_f}{\operatorname{argmin}} g(\mathbf{x}). \tag{5}$$

See Fig. 3 (b). The starting point of the second optimization is P^*. This local optimization is performed at fixed radius value with a gradient algorithm and hence relatively cheap in terms of lsf evaluation.

Depending on the shape of the failure region and the important ring, the representative point is thus either the starting point P^* of this failure region in the important ring (Case 1) or the most negative point $\tilde{P}^*$ at the lower bound of the important ring for failure regions starting before the important ring (Case 2), as illustrated in Fig. 3.

To find all the failure regions, these optimizations are repeated with a random multi-start technique. The resulting local minima P^* or $\tilde{P}^*$ representing the failure regions of the systems are gathered in a set L. It may happen that some points represent the same failure region. To select a first failure region for sampling, the representative points of the set L are ranked and sorted. In Case 1, representative points P^* of failure regions are ranked according to their norm $\|P^*\| > \text{LB}$. In Case 2, representative points $\tilde{P}^*$ of failure regions are ranked according to the value of their lsf $g(\tilde{P}^*) < 0$, as their norms are equal to LB. The set L is then sorted in ascending order with regard to the ranking value of each representative point. It should be noted that the representative points of Case 2 whose ranking values are negative are necessarily ranked before those of Case 1 whose ranking values are positive. A first failure region is then identified with the first point P_1 of the ordered set L. This point is thus the closest to the origin and its lsf evaluation is the most negative if its norm is equal to LB. The identification problem is summarized in Algorithm 1.

2.3. Sampling problem: Construction of the auxiliary density for the failure region

To generate more observations in the failure region found in the previous section, an auxiliary density is built step by step with optimized parameters as per the sampling problem introduced above. Taking advantage of the stochastic decomposition of the elliptical inputs, the

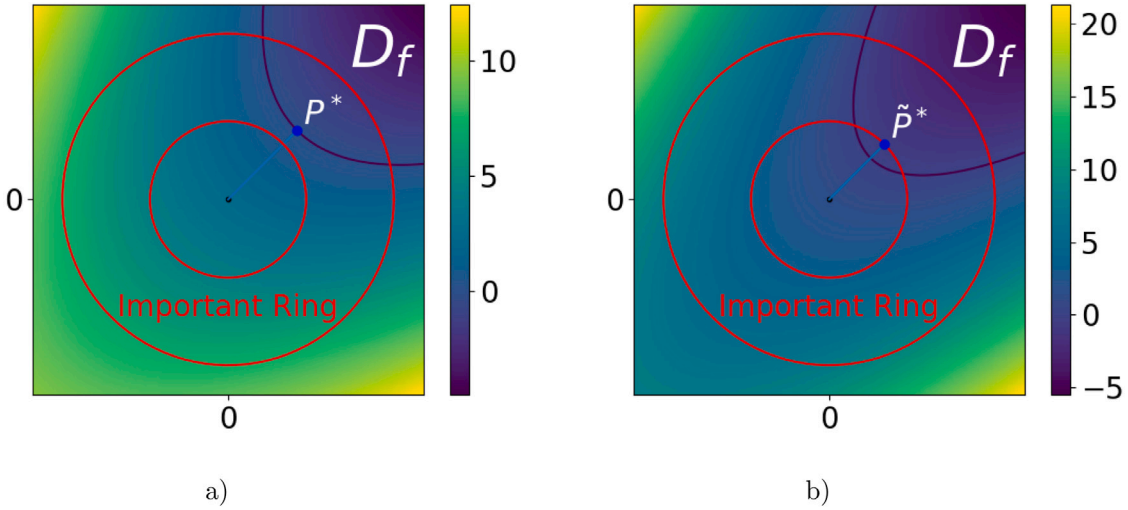

Fig. 3. Illustration of the failing point representative of the failure region P^* in (a) Case 1 and $\tilde{P}^*$ in (b) Case 2. The blue line represents the Euclidean distance between the representative point and the origin. The red circles delineate the lower bound and upper bound of the important ring. In both examples, there is only one failure region in the failure domain, located in the upper right corner delimited in black.

Algorithm 1 Identification Problem

Require: The lsf g and its gradient ∇g.

Initialization

The set L is empty. Generate a random vector $\mathbf{V}$ of starting points $\mathbf{X}_0$.

Multi-start local optimizations

for $\mathbf{X}_0 \in \mathbf{V}$ **do**

Search for the closest failing point with Eq. (4) with starting point $\mathbf{X}_0$. The result is P^*.

if $\|P^*\| = \text{LB}$ **then**

The failure region starts before the important ring: This is Case 2. Perform the optimization given in Eq. (5), with starting point P^*, to find the most negative point in the LB. The result is $\tilde{P}^*$. Add the representative point $\tilde{P}^*$ to the set L, with associated ranking value $g(\tilde{P}^*)$.

else

The closest failing point is inside the important ring: This is Case 1. Add the representative point P^* to the set L, with associated ranking value $\|P^*\|$.

end if

end for

Identification of a first failure region

Sort the set L in ascending order with respect to the ranking value of each representative point. Identify P_1 as the first point of the ordered set L.

return The ordered set L and a first identified failure region with P_1.

parametric IS density used to sample in the failure region is constructed as the product of a density h_R on the random variable R and a density $h_{\mathbf{T}}$ on the random vector $\mathbf{T}$.

The selected radial distribution h_R is the original law of R, conditional on being greater than a scalar parameter $r_{\text{opt}} \in \mathbb{R}_+$, viz.

$$h_R(r; r_{\text{opt}}) = f_{R|R>r_{\text{opt}}}(r) = \mathbb{I}_{R>r_{\text{opt}}}(r) f_R(r)/\mathbb{P}(R > r_{\text{opt}}).$$

This choice of distribution for the radial component, which excludes part of the original distribution, is close to what is achieved in RBIS [23,24], where its efficiency is underlined.

The selected directional distribution $h_{\mathbf{T}}$ is a vMF distribution, a choice already proven to be efficient in [26,32,33]. It depends on two parameters, namely the concentration parameter $\kappa \in \mathbb{R}_+$ and the mean direction parameter $\boldsymbol{\nu} \in \mathcal{T}_d = \{(t_1, \dots, t_d) \in \mathbb{R}^d : t_1^2 + \cdots + t_d^2 = 1\}$ of dimension d. Specifically,

$$h_{\mathbf{T}}(\mathbf{t}; \kappa, \boldsymbol{\nu}) = c_d(\kappa) e^{\kappa \boldsymbol{\nu}^\top \mathbf{t}} \quad \text{with} \quad c_d(\kappa) = \frac{\kappa^{d/2-1}}{(2\pi)^{d/2} I_{d/2-1}(\kappa)},$$

where $I_{d/2-1}$ denotes the modified Bessel function of the first kind of order $d/2-1$. If $\kappa = 0$, this boils down to the uniform distribution on $\mathcal{T}_d$. As κ grows, the distribution is more and more concentrated around the mean direction $\boldsymbol{\nu}$.

The choice of these parametric densities leads to a total of $d+2$ scalar parameters to be set. For the first failure region identified above with P_1, the goal is thus to find the optimal parameters $r_{\text{opt},1}, \kappa_1$ and $\boldsymbol{\nu}_1$ such that the density $h_R(r; r_{\text{opt},1}) \times h_{\mathbf{T}}(\mathbf{t}; \kappa_1, \boldsymbol{\nu}_1)$ is close to the optimal density of this failure region, viz.

$$h_{\text{opt},1}(r, \mathbf{t}) = \mathbb{I}_{D_{f,1}}(r\mathbf{t}) f_R(r) f_{\mathbf{T}}(\mathbf{t}) / P_{f,1},$$

where $D_{f,1}$ denotes the failure domain of this particular failure region and $P_{f,1}$ its probability. Instead of optimizing the parameters $r_{\text{opt},1}$, κ_1, and $\boldsymbol{\nu}_1$ of dimension $d+2$ with a Cross-Entropy (CE) algorithm as in [33], one can take advantage of the coordinates of the optimized point P_1 representative of the failure region as derived below. This simplifies the optimization of the parameters.

The parameter $r_{\text{opt},1}$ defines the minimum value of R such that $R\mathbf{T}$ belongs to $D_{f,1}$, for all $\mathbf{T}$. Depending on the location of the failure region compared to the important ring, $r_{\text{opt},1}$ is set differently. Using the same notation as in Section 2.2 with Cases 1 and 2, the settings of $r_{\text{opt},1}$ are as follows:

Case 1: Set $r_{\text{opt},1} = \|P_1\|$. Indeed, P_1 is the closest failing point in the important ring. No point whose norm is below $r_{\text{opt},1}$ can be in the failure region of the important ring.

Case 2: The norm of P_1 equals the distance between the origin and the lower bound of the important ring. Thus, $r_{\text{opt},1}$ is set to 0 to avoid any bias, given that additional information on the radial component of the failure region is not available. Therefore, the distribution of the variable R is left unchanged in this particular case.

The mean direction $\boldsymbol{\nu}_1$ is set to be the direction of P_1, viz. $\boldsymbol{\nu}_1 = P_1/\|P_1\|$. This decision implies that the direction of the point P_1 is where the likelihood of the density $h_{\mathbf{T}}$ is largest. It makes it possible to set the value of the vector $\boldsymbol{\nu}_1$ of dimension d directly with the coordinates of P_1, which are available after the optimizations of the identification problem described in Section 2.2.

Selecting the direction of P_1 as the most important direction for this failure region is relevant both in Cases 1 and 2. Indeed in Case 1, P_1 is the design point; thus, selecting its direction as the most important is close to what is done in line sampling [5], where the efficiency of this choice has already been underlined. In Case 2, given that the evaluation of P_1 with the lsf has the most negative value in the lower bound LB of the important ring, the direction of P_1 is the most likely to be well centered with regard to the location of the failure region.

Finally, the scalar κ_1 is set as the result of a Cross-Entropy based Adaptive IS method (CE-AIS) [35,36]. CE-AIS is a sampling method allowing to optimize sequentially the parameters of an IS density in order to get as close as possible to the optimal IS density. To do so, it minimizes the Kullback–Leibler (KL) divergence between the parametric density and the optimal IS density. Here, the parameter κ has to minimize the KL distance between the optimal IS density $h_{\text{opt},1}(r,\mathbf{t})$ of this particular failure region and the product density $h_R(r;r_{\text{opt},1}) \times h_{\mathbf{T}}(\mathbf{t};\kappa,\boldsymbol{\nu}_1)$. After some calculations, see [33], one finds that the optimization problem is given by the following equation:

$$\kappa_1 = \underset{\kappa}{\text{argmax}} \left[\int_{\mathbb{R}_+} \int_{\mathcal{T}_d} \frac{1}{P_{f,1}} \mathbb{I}_{D_{f,1}}(r\mathbf{t}) f_{\mathbf{T}}(\mathbf{t}) f_R(r) \ln\left\{ h_R(r;r_{\text{opt},1}) \times h_{\mathbf{T}}(\mathbf{t};\kappa,\boldsymbol{\nu}_1) \right\} \mathrm{d}r\mathrm{d}\mathbf{t} \right].$$

The probability $P_{f,1}$ being a constant, it can be ignored; the same holds for the h_R density in the logarithm, which does not depend on κ. This integral is then estimated by a Monte Carlo method, viz.

$$\kappa_1 \approx \underset{\kappa}{\text{argmax}} \frac{1}{M} \sum_{\ell=1}^{M} \mathbb{I}_{D_{f,1}}(R_\ell \mathbf{T}_\ell) \ln\{h_{\mathbf{T}}(\mathbf{T}_\ell;\kappa,\boldsymbol{\nu}_1)\}, \quad R_\ell \sim f_R, \quad \mathbf{T}_\ell \sim f_{\mathbf{T}}.$$

Introducing an IS density h_{CE} for the computation of the above, one can write

$$\kappa_1 \approx \underset{\kappa}{\text{argmax}} \frac{1}{M} \sum_{\ell=1}^{M} \mathbb{I}_{D_{f,1}}(R_\ell \mathbf{T}_\ell) \ln\{h_{\mathbf{T}}(\mathbf{T}_\ell;\kappa,\boldsymbol{\nu}_1)\} \frac{f_R(R_\ell) f_{\mathbf{T}}(\mathbf{T}_\ell)}{h_{\text{CE}}(R_\ell \mathbf{T}_\ell)}, \quad R_\ell \mathbf{T}_\ell \sim h_{\text{CE}}. \tag{6}$$

Were the indicator function of the failure domain and the IS likelihood ratio to be removed, this optimization would be exactly the same as a maximum likelihood estimation (MLE) of the vMF distribution parameters, when $\boldsymbol{\nu}$ is known. With the indicator function and the IS likelihood ratio, the optimization (6) becomes a weighted MLE problem whose solution is known. After some calculations using formulas from [27,32], the optimal κ_1 is found to be the solution of the equation

$$\frac{I_{d/2}(\kappa_1)}{I_{d/2-1}(\kappa_1)} = \frac{\mathbf{r}^\top \boldsymbol{\nu}_1}{\sum_{\ell=1}^{M} \mathbb{I}_{D_{f,1}}(R_\ell \mathbf{T}_\ell) f_R(R_\ell) f_{\mathbf{T}}(\mathbf{T}_\ell)/h_{\text{CE}}(R_\ell \mathbf{T}_\ell)}, \tag{7}$$

where

$$\mathbf{r} = \sum_{\ell=1}^{M} \mathbb{I}_{D_{f,1}}(R_\ell \mathbf{T}_\ell) \frac{f_R(R_\ell) f_{\mathbf{T}}(\mathbf{T}_\ell)}{h_{\text{CE}}(R_\ell \mathbf{T}_\ell)} \mathbf{T}_\ell .$$

As one cannot solve Eq. (7) analytically, it is proposed in [27] to approximate κ_1 with $\kappa_1 \approx (\xi d - \xi^3)/(1-\xi^2)$, where $\xi = I_{d/2}(\kappa_1)/I_{d/2-1}(\kappa_1)$. If κ_1 happens to be negative, then it is set to 0. With these equations, the value of κ_1 is gradually updated with the convergence of a CE-AIS algorithm as follows.

1. Initialization. Starting from a value $\kappa_{1,0} \neq 0$, a sample S_0 of size N is generated from $h_R(r,r_{\text{opt},1}) \times h_{\mathbf{T}}(\mathbf{t},\kappa_{1,0},\boldsymbol{\nu}_1)$. With this sample, the failure probability of this region is estimated by

$$\hat{P}_{f,1,0} = \frac{1}{N} \sum_{i=1}^{N} \mathbb{I}_{D_{f,1}}(R_i \mathbf{T}_i) \frac{f_R(R_i) f_{\mathbf{T}}(\mathbf{T}_i)}{h_{\text{CE},0}(R_i \mathbf{T}_i)}, \tag{8}$$

where

$$h_{\text{CE},0} = h_R(r;r_{\text{opt},1}) \times h_{\mathbf{T}}(\mathbf{t};\kappa_{1,0},\boldsymbol{\nu}_1).$$

The theoretical CV of $\hat{P}_{f,1,0}$, given by Eq. (2) and denoted CV_0, is estimated, and $\kappa_{1,1}$ is computed with population S_0, density $h_{\text{CE},0}$, and Eqs. (7). Set $p = 1$.

It is assumed that $\mathbb{I}_{D_{f,1}}(R_i\mathbf{T}_i) = \mathbb{I}_{D_f}(R_i\mathbf{T}_i)$ while the observations are generated with $\kappa_{1,p} \neq 0$ around $\boldsymbol{\nu}_1$. Thus in Eqs. (7), (8) and (9), no distinction is made between those two failure domains. The situation where not a single $R_i\mathbf{T}_i$ from S_0 is failing may occur in two different settings. First, if the initial $\kappa_{1,0}$ is too small, then the observations are not concentrated enough around $\boldsymbol{\nu}_1$ and with a particularly narrow failure region, $\mathbb{I}_{D_{f,1}}(R_i\mathbf{T}_i) = 0$ for all S_0. Second, if the failure region associated with P_1 is extremely small, then even with a large $\kappa_{1,0}$ all points of S_0 may belong to the safety domain. For both of these situations the cross-entropy optimization is stopped and the failure region associated to P_1 is considered negligible for the estimation of the failure probability.

2. Updating of the concentration parameter. While $\text{CV}_{p-1} \geq 10\%$, a sample S_p of size N is generated from $h_R(r;r_{\text{opt},1}) \times h_{\mathbf{T}}(\mathbf{t};\kappa_{1,p},\boldsymbol{\nu}_1)$. The failure probability of this region is estimated from the $p+1$ samples generated, viz. $S_0,\ldots,S_p$, using the following adaptive MIS estimate:

$$\hat{P}_{f,1,p} = \frac{1}{N(p+1)} \sum_{i=1}^{N(p+1)} \mathbb{I}_{D_{f,1}}(R_i\mathbf{T}_i) \frac{f_R(R_i) f_{\mathbf{T}}(\mathbf{T}_i)}{h_{\text{CE},p}(R_i\mathbf{T}_i)}, \tag{9}$$

where

$$h_{\text{CE},p} = h_R(r;r_{\text{opt},1}) \times \frac{1}{p+1} \sum_{u=0}^{p} h_{\mathbf{T}}(\mathbf{t};\kappa_{1,u},\boldsymbol{\nu}_1).$$

The theoretical CV of $\hat{P}_{f,1,p}$, denoted CV_p, is estimated and the $\kappa_{1,p+1}$ is updated with samples $S_0,\ldots,S_p$, density $h_{\text{CE},p}$, and Eq. (7). The parameter p is then incremented to $p+1$. This step is repeated until $\text{CV}_{p-1} < 10\%$.

3. End of the algorithm. Once the CV convergence criterion is reached, set $n_1 = p$. A last sample S_{n_1} of size N is generated from $h_R(r;r_{\text{opt},1}) \times h_{\mathbf{T}}(\mathbf{t};\kappa_{1,n_1},\boldsymbol{\nu}_1)$.

Updating $\kappa_{1,p+1}$ with all the previous samples, rather than just the last one S_p in Step 2, proved to be more efficient in terms of stability of the κ value and leads to a faster convergence of the algorithm. The matrix M_1 is defined as the vector $M_1 = (S_0,\ldots,S_{n_1})$ of all the generated samples.

The accurate computation of the coordinates of P_1 with the local optimization problems of Section 2.2 is thus crucial. Indeed, a greater number of iterations in the CE-AIS algorithm could be required to reach the CV convergence criterion if the mean direction $\boldsymbol{\nu}_1$ or $r_{\text{opt},1}$ are inaccurate. This would lead to a larger simulation budget.

At the end of the algorithm, the density $h_R(r;r_{\text{opt},1}) \times h_{\mathbf{T}}(\mathbf{t};\kappa_{1,n_1},\boldsymbol{\nu}_1)$ is close to $h_{\text{opt},1}$ and is the best density with this parametric setting to sample the failure region. Nevertheless, each intermediate density $h_R(r;r_{\text{opt},1}) \times h_{\mathbf{T}}(\mathbf{t};\kappa_{1,p},\boldsymbol{\nu}_1)$ and its corresponding sample S_p are also kept and used in the final MIS estimate. This improves the accuracy of the probability estimate in terms of empirical CV. Also, it allows for a better use of all the evaluations of the expensive limit state function g.

2.4. Adaptation step to take into account the failure region modeled

Once a first failure region has been identified and sampled, the search for the remaining failure regions can be initiated. As mentioned at the beginning of Section 2.2, the search for the failure regions is greatly inspired by the FORM method for multiple failure modes [8]. In this method, once a failure region is found, a bulge, denoted by Bulge_1, is built around the location of its associated representative failing point P_1 and added to the lsf g. The modified limit state function, written $\tilde{g}$, is then

$$\tilde{g}(\mathbf{x}) = g(\mathbf{x}) + \text{Bulge}_1(\mathbf{x}),$$

and the modified failure domain is written $\tilde{D}_f = \{r\mathbf{t} : \tilde{g}(r\mathbf{t}) \leq 0\}$. This failure region is thus not considered again in the search for the

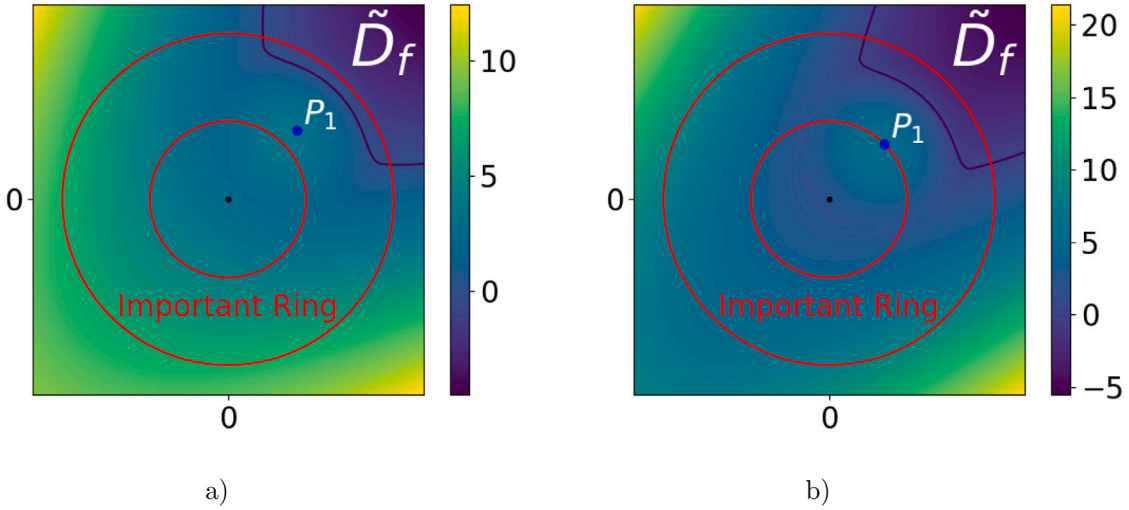

Fig. 4. Illustration of the bulge built around the representative point P_1 of the failure region and the resulting modified failure domain $\tilde{D}_f$ in (a) Case 1 and (b) Case 2. This illustration should be compared to Fig. 3 for a better understanding. The red circles represent the lower bound and upper bound of the important ring. In both examples, there is only one failure region in the failure domain, located in the upper right corner delimited in black.

remaining failure regions, as it belongs to the safety domain. The same process is employed here with some adjustments; it is the adaptation step introduced above.

In the proposed method, two different situations have been defined as Case 1 and Case 2 depending on the location of the failure region within the important ring. Given that the value of the lsf at the failing point $g(P_1)$ is not equal to zero in Case 2, a small modification has been added to the classical bulge equation presented in [8] to introduce a bulge equation that suits both situations:

$$\text{Bulge}_1(\mathbf{x}) = \begin{cases} s_1 \left(\alpha_1^2 - \|\mathbf{x} - P_1\|^2\right)^2 & \\ -\mathbb{I}_{g(P_1)<0} \dfrac{g(P_1)}{\alpha_1} \left(\alpha_1 - \|\mathbf{x} - P_1\|\right) & \text{if } \|\mathbf{x} - P_1\| \leq \alpha_1, \\ 0 & \text{elsewhere,} \end{cases}$$

where $\mathbb{I}_{g(P_1)<0} = 1$ when $g(P_1) < 0$ and 0 otherwise. The resulting modified failure regions in those two situations are displayed in Fig. 4.

The scalar α_1 is the radius of the bulge defined by $\alpha_1 = \gamma \times \beta_1$ and s_1 is the scale of the bulge, defined by

$$s_1 = \frac{\delta\beta_1 \|\nabla g(P_1)\|}{\left\{(\gamma\beta_1)^2 - (\delta\beta_1)^2\right\}^2},$$

where $\delta = 0.75$ and $\gamma = 1.1$ as in [8], and $\beta_1 = \|P_1\|$. Any point in the bulge is thus no longer in the updated failure domain $\tilde{D}_f$. A first updating of the ordered set L is made to remove any of those points.

In Case 2, P_1 is located on the lower bound of the important ring and hence $\beta_1 = \text{LB}$. However, most of the observations generated are not located around P_1. Indeed, as the distribution of the radial component R is left unchanged (see Section 2.3), most observations have a radial value closer to the mean value of R than LB. Therefore, the bulge built around P_1 is not representative of the samples generated in this failure region. A failing point belonging to the same failure region as P_1 may be found at a distance from P_1 superior to α_1.

In Case 1, the same situation may happen if the radius α_1 of the bulge is not large enough. Thus another criterion, inspired by the angle criterion in [8], is introduced for both Case 1 and Case 2 in order to prevent this phenomenon: the maximum angle ϕ_1 between P_1 and the failing points of the population M_1 is estimated and the failing cone C_1 associated to P_1 is defined as $C_1 = \{\mathbf{x} : \widehat{\mathbf{x}P_1} \leq \gamma \times \phi_1\}$. Any failing point belonging to this cone is representative of the same failure region and must also be removed from the ordered set L to avoid redundancy.

After this second updating, if the ordered set L is not empty, then the remaining points represent some failure regions that are different from the first one and need to be considered. The next failure region is identified with the first point of the updated ordered set L, denoted as P_2. The sampling problem (Section 2.3) is then repeated with this failure region represented by P_2. The failure domain used in the sampling problem is still $D_f = \{r\mathbf{t} : g(r\mathbf{t}) \leq 0\}$ without the modification $\tilde{g}$ defined above. It prevents introducing a bias in the probability estimation. At the end of the sampling problem, the second failure region around P_2 has been properly sampled and another auxiliary density has been iteratively constructed. A second bulge Bulge_2 is created in the same way as Bulge_1, so that $\tilde{g}$ is updated again. The ordered set L is also updated with the distance criterion α_2 and the cone criterion C_2.

This scheme goes on until the set L is empty, with the number of failure regions found equal to k. Algorithm 2 sums up the process of sampling in all failure regions represented by points in the set L. The modified lsf is initialized with $\tilde{g} = g$ and the number of failure regions k is initialized with $k = 0$ as there is no identified failure region at the start of the algorithm.

Algorithm 2 Sampling in all failure regions of the ordered set L

Require: The ordered set L, the lsf g, the modified lsf $\tilde{g}$ and the number k of failure regions.
Construction of densities and sampling
while $L \neq \emptyset$ **do**
Set $k = k + 1$. Select P_k as the first element of the ordered set L.
Sampling Problem: Construct an optimal auxiliary density for the failure region represented by P_k and generate a population M_k in this failure region as in Section 2.3.
Adaptation Step: Add the Bulge_k to the modified lsf $\tilde{g}$ and update the set L by removing points closer to α_k from P_k and belonging to the cone C_k.
end while
All the failure regions represented by failing points in the set L have been sampled.
return The number k of failure regions and the modified lsf $\tilde{g}$.

2.5. Search for missed failure regions

The set L found in the identification problem presented in Section 2.2 may not include all the existing failure regions. For example, one failure region may be so dominant that all the optimized points

of the set L have converged to this particular region. Therefore, some failure regions that are slightly harder to find by optimization may be missed. To solve this problem, another set of optimizations is performed, to find the failure regions that could have been overshadowed. The optimizations are the same as the ones presented in Section 2.2 with Eqs. (4) and (5) except for two updates. First, the failure domain is no longer D_f but the modified one $\tilde{D}_f = \{r\mathbf{t} : \tilde{g}(r\mathbf{t}) \leq 0\}$. Thereby, all the bulges constructed earlier prevent the optimization from converging back to the same points, because they are no longer in the failure domain. Second, the multi-start technique of the first optimization (4) is centered around the opposite direction $\mathbf{x}_0$ of the failing points previously found, as suggested in the FORM method with multiple design points [8], viz.

$$\mathbf{x}_0 = -\epsilon(P_1 + \cdots + P_k), \tag{10}$$

where $\epsilon = 0.5$. After the optimizations, a new set L is found. The failing points of this set are all located at least α_i-away from each point P_i with $i \in \{1, \ldots, k\}$. After removing the failing points of the set belonging to the cone C_i of each P_i, the set L contains only failing points representative of failure regions that have not been sampled yet. It is sorted as described in Section 2.2. Algorithm 2 is then repeated for this ordered set L until is it empty. Algorithm 3 sums up the sampling of all failure regions of the failure domain.

Algorithm 3 Search and sampling of all failure regions of the failure domain

Require: The lsf g and its gradient ∇g.

Initialization

Identification Problem: Create an ordered set L as output of the Algorithm 1 with inputs $(g, \nabla g)$.

Set the number of failure region $k = 0$. Initialize the modified lsf with $\tilde{g} = g$

Sampling all failure regions represented by failing points in the set L

while $L \neq \emptyset$ **do**

Sampling Problem and Adaptation Step: Generate a sample in every failure region represented by failing points in the ordered set L as derived in Algorithm 2 with inputs $(L, g, \tilde{g}, k)$ and outputs $(k, \tilde{g})$.

Identification Problem: Create a new set L with the optimizations presented in Section 2.2 with the modified lsf $\tilde{g}$ and failure domain $\tilde{D}_f = \{r\mathbf{t} : \tilde{g}(r\mathbf{t}) \leq 0\}$ and $\mathbf{x}_0 = -\epsilon(P_1 + \cdots + P_k)$. Update this set L by removing points located within the cones C_i for each P_i with $i \in \{1, \ldots, k\}$ and sort the set L.

end while

All failure regions of the failure domain have been identified and sampled.

Set K equal to the last value of k, such that K is the final number of failure regions identified and sampled, in the failure domain.

return The total number of failure regions K.

The algorithm ends when the new set L is found to be the empty set. It means that no other failure region has been found, i.e., the entire failure domain has (presumably) been covered. The bulges keep getting added to the modified lsf $\tilde{g}$ through the different created sets L. It is recalled here that the modified limit state function is used only for the optimizations performed in the identification problems, and not for the construction of the auxiliary densities in the sampling problems.

2.6. Estimation of the global failure probability

The global failure probability is estimated at the end of Algorithm 3 with the MIS estimate presented before. The global IS auxiliary density is a mixture of a number n_{total} of densities structured as $h_R \times h_{\mathbf{T}}$. The final form of the estimate is

$$\hat{P}_f^{\text{MIS}} = \frac{1}{n_{\text{total}} \times N} \sum_{i=1}^{n_{\text{total}} \times N} \mathbb{I}_{D_f}(R_i \mathbf{T}_i) \frac{f_R(R_i) f_{\mathbf{T}}(\mathbf{T}_i)}{h_{\text{MIS}}(R_i \mathbf{T}_i)}, \quad R_i \mathbf{T}_i \sim h_{\text{MIS}}$$

with

$$h_{\text{MIS}}(r\mathbf{t}) = \frac{1}{n_{\text{total}}} \sum_{j=1}^{K} h_R(r; r_{\text{opt},j}) \left\{ \sum_{\ell=0}^{n_j} h_{\mathbf{T}}(\mathbf{t}; \kappa_{j,\ell}, \boldsymbol{\nu}_j) \right\}.$$

Thus $N_{\text{samp}} = n_{\text{total}} \times N$. As previously noted, the number n_{total} of IS auxiliary densities is equal to $n_1 + \cdots + n_K + K$. This estimate does not require any prior knowledge of the number K of failure regions, as it is computed within the algorithm. The lsf g is evaluated through several repetitions of the identification problem (Section 2.2) and the sampling problem (Section 2.3). The numbers $N_{\text{opt},1}$ and $N_{\text{opt},2}$ denote the global numbers of evaluations of g and ∇g, respectively, required for all the optimizations performed in the identification problems, and N_{samp} is the final number of lsf evaluations required in the sampling problems. The total number of lsf evaluations is equal to $N_{\text{opt},1} + N_{\text{samp}}$. If there exist some errors in the gradient estimation or in the local optimizations performed during the identification steps, the identification of the different failure regions and the coordinates of their corresponding representative point can be impacted. The resulting MIS probability estimate may be biased if the parameters $r_{\text{opt},i}$ are not identified well. Also, a greater simulation budget may be required to reach the CV convergence criterion of the CE-AIS algorithm if the sampling density is sub-optimal because of inaccurate mean direction $\boldsymbol{\nu}_i$ or $r_{\text{opt},i}$.

To clarify the procedure, an example in dimension 2 is presented next. This example is meant to be for illustrative purposes only, as the goal of the algorithm is to estimate the failure probability of systems involving a large number of input variables.

Example in dimension 2: A 4-branch system

The following example is frequently used in the literature [10,33]. The inputs are assumed to be Gaussian, viz. $\mathbf{X} \sim \mathcal{N}(\mathbf{0}_2, \mathbf{I}_2)$, and the lsf equation is given by

$$g(\mathbf{X}) = \min \begin{Bmatrix} (X_1 - X_2)^2/10 - (X_1 + X_2)/\sqrt{2} + 3, \\ (X_1 - X_2)^2/10 + (X_1 + X_2)/\sqrt{2} + 3, \\ (X_1 - X_2) + 7/\sqrt{2}, \\ (X_2 - X_1) + 7/\sqrt{2} \end{Bmatrix}.$$

The reference value for the failure probability is 2.22×10^{-3}. Fig. 5 displays the function g and the contour of the failure domain.

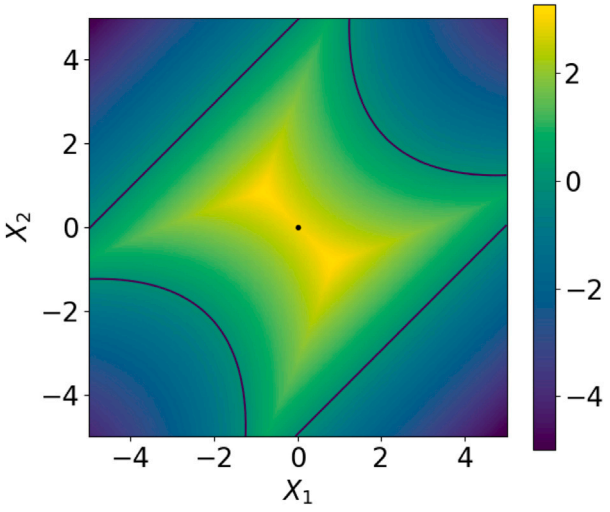

Fig. 5. Limit state function for the 4-branch system. This system has four failure regions located at the four corners of the input space; the failure domain is delimited in black.

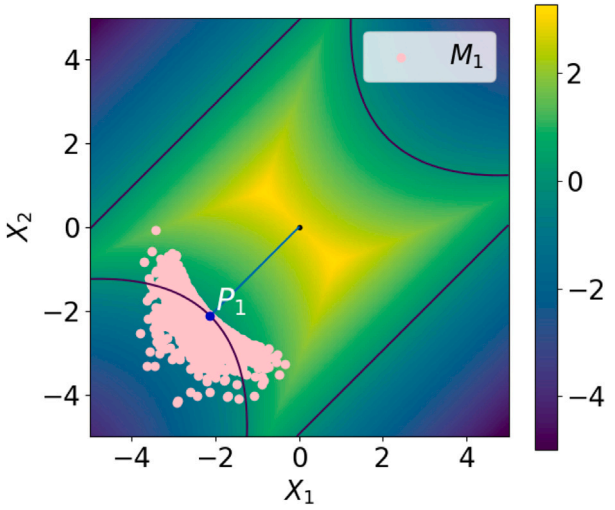

Fig. 6. Sampling of the first failure region of the 4-branch system. One has $P_1 = (-2.12, -2.12)$, $r_{\text{opt},1} = 2.99$ and $\boldsymbol{\nu}_1 = (-0.71, -0.71)$. The population M_1 is of size $2N$ as only two iterations were needed in the algorithm, with $\kappa_{1,0} = 20$ and $\kappa_{1,1} = 33.5$.

The first step of the algorithm is to find P_1 through optimization (Section 2.2); this is the identification problem. Here the dimension is too low for the important ring to be any restrictive; it encompasses the whole input space. Hence, the failure regions all start inside the important ring. This application is thus an example of the situation referred to as Case 1 in the previous sections. After this identification problem, the set L contains only three different representative points, viz. $(-2.12, -2.12)$, $(2.12, 2.12)$ and $(2.47, -2.47)$. The Euclidean norm of both $(2.12, 2.12)$ and $(2.12, -2.12)$ is very close to 3 while the Euclidean norm of $(2.47, -2.47)$ is close to 3.5; thus it is last in the ordered set. This first identification problem has missed the fourth failure region.

The first point of the set is $P_1 = (-2.12, -2.12)$ with $r_{\text{opt},1} = 2.99$ and $\boldsymbol{\nu}_1 = (-0.71, -0.71)$. The sampling of the failure region around P_1 is performed (sampling problem, Section 2.3) with $\kappa_{1,0} = 20$ and $N = 1000$. The first CV_0 computed is equal to 2.6%, thus κ is only updated once and its final value is 33.5. The population M_1 of size $2N$ is illustrated in Fig. 6.

The Bulge_1 is added to the limit state function g to create the modified lsf $\tilde{g}$ and the set L is updated (adaptation step). The same scheme is repeated for $P_2 = (2.12, 2.12)$ and $P_3 = (2.47, -2.47)$ (Section 2.4). Populations M_2 and M_3 are displayed in Fig. 7. The set L is empty at this point, and the search for missed failure regions begins (identification problem, Section 2.5) with a new set L resulting from the optimization on the modified limit state function $\tilde{g}$, displayed in Fig. 8.

The new set L results in the singleton $\{(-2.47, 2.47)\}$. The sampling of the fourth failure region is performed (sampling problem), Bulge_4 is added to $\tilde{g}$ and once this is done, the set L is empty (adaptation step). The resulting population M_4 is displayed in Fig. 9 with the new modified lsf.

The new set L resulting from the optimization fails to detect any failure region different from the ones previously found (identification problem) and thus the algorithm stops. The failure probability is estimated with a MIS estimate of eight densities, two for each failure region. The estimated probability is equal to 2.23×10^{-3}, with a theoretical CV equal to 1.3%. The total number of evaluations of the gradient of g for the optimizations of the identification problems is equal to $N_{\text{opt},2} = 330$. The number of evaluations of g comprises $N_{\text{opt},1} = 476$ evaluations for the optimizations of the identification problems, and $N_{\text{samp}} = 4 \times 2 \times 1000 = 8000$ for the sampling problems of the four failure regions.

3. Numerical investigations with high-dimensional input space

The performance of the proposed algorithm was investigated with three numerical examples taken from the IS literature and with a realistic engineering application taken from the aviation industry. The first two were compared with the improved Cross-Entropy vMF-Nakagami Mixture algorithm (iCE-vMFNM) of [33] and with a subset simulation (SS) algorithm [15]. SS algorithms are known to be efficient in high-dimensional input space [38]. The Monte Carlo method was used for reference value. The inputs of the first two examples and the realistic engineering application follow the standard Gaussian distribution, while the inputs of the third example follow a multivariate Student distribution.

As previously noted, all the examples involve inputs of dimension 100 and above. Nevertheless, as shown at the end of the previous section, the algorithm can also perform well in small dimension, even though it is not the primary objective of the proposed method.

The first example is a series system problem with four components for which the number of random variables can be chosen without affecting the probability of failure; it was inspired by a numerical application from [32,33]. The second example has to do with a Duffing oscillator under a random loading as considered in [39]. The third example pertains to a large portfolio comprising loans that are subject to possible default, with $d = 250$, taken from [40–42]. The last example concerns the drag coefficient of an airfoil in inviscid transonic flow subject to random shape distortion [43], with $d = 100$.

Optimization was performed with the SLSQP algorithm [44]. The random vector for the multi-start technique mentioned in the search for the failure regions was generated with a Latin Hypercube Sampling (LHS) [45] of size 10. This sampling ensures that 10 random starting points are well distributed over the entire input space. Although the choice of 10 for the sampling size is arbitrary, it proved to be sufficient for the examples considered here.

For the CE-AIS method, N was always set to 1000 and the maximum number of iterations was set to $p_{\max} = 10$ except for the last application, where it is set to 5. The number $p_{\max}$ is rather low, but it is adequate as the only updated parameter is the scalar κ. In the first example, a study of the best initial value of $\kappa_{i,0}$ in the CE-AIS method was performed. For the iCE-vMFNM algorithm, the maximum number of iterations in the CE method was also set to 10 for comparison purposes and the parameters K and $\text{CV}_{\text{target}}$ were optimally set for each application. For the SS algorithm, the maximum number of iterations was also set to 10, while the quantile parameter ρ equals 0.1. To compare the different methods, 500 independent simulation runs were performed to calculate the statistics of the probability estimates and the other quantities of interest, except for the last example where the algorithm ran only once.

3.1. Series system of four linear lsfs

The first example demonstrates the robustness of the proposed algorithm to find all the failure regions in the high-dimensional input space. It is defined by a series system of four linear lsfs in the standard Gaussian space $\mathbf{X} \sim (\mathbf{0}_d, \mathbf{I}_d)$. The lsf is given by

$$g_1(\mathbf{X}) = \min \left\{ \begin{array}{c} \beta + \frac{1}{\sqrt{d}} \sum_{i=1}^{d} X_i, \\ \beta - \frac{1}{\sqrt{d}} \sum_{i=1}^{d} X_i, \\ \beta + \frac{1}{\sqrt{d}} \left(\sum_{i=1}^{d/2} X_i - \sum_{i=d/2+1}^{d} X_i \right), \\ \beta + \frac{1}{\sqrt{d}} \left(-\sum_{i=1}^{d/2} X_i + \sum_{i=d/2+1}^{d} X_i \right) \end{array} \right\}.$$

The failure probability is then independent of the number d of random variables. In order to have a low failure probability, it was

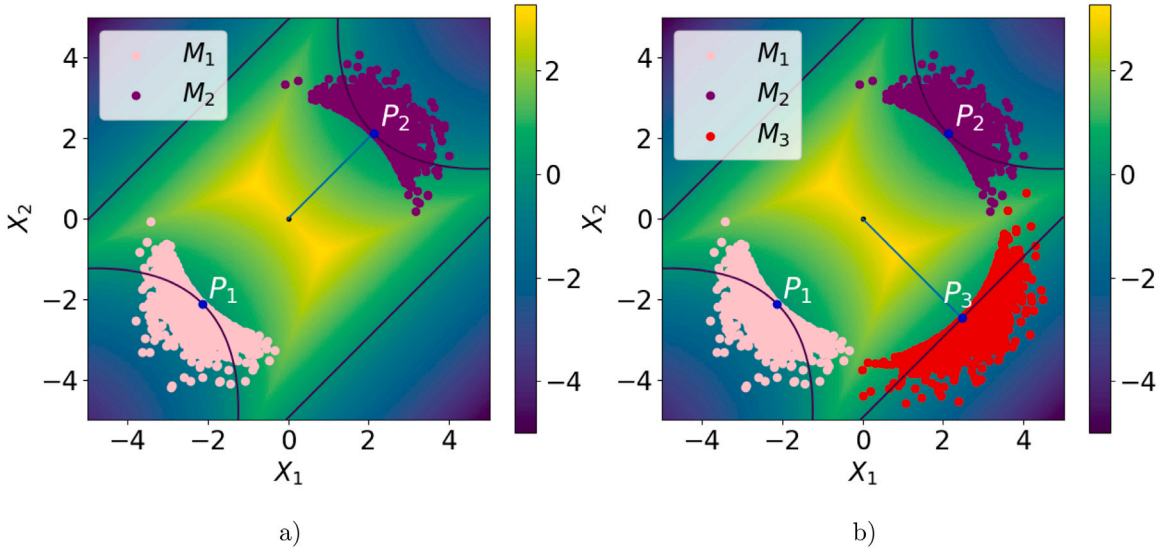

Fig. 7. Sampling of (a) the second and (b) third failure regions of the 4-branch system. One has $P_2 = (2.12, 2.12)$, $r_{\text{opt},2} = 2.99$, and $\boldsymbol{\nu}_2 = (0.71, 0.71)$. Population M_2 is of size $2N$ as only two iterations were needed in the algorithm, with $\kappa_{2,0} = 20$ and $\kappa_{2,1} = 27.6$. Moreover, $P_3 = (2.74, -2.47)$, $r_{\text{opt},3} = 3.49$, and $\boldsymbol{\nu}_3 = (0.71, -0.71)$. Population M_3 is of size $2N$ as only two iterations were needed in the algorithm, with $\kappa_{3,0} = 20$ and $\kappa_{3,1} = 18.1$.

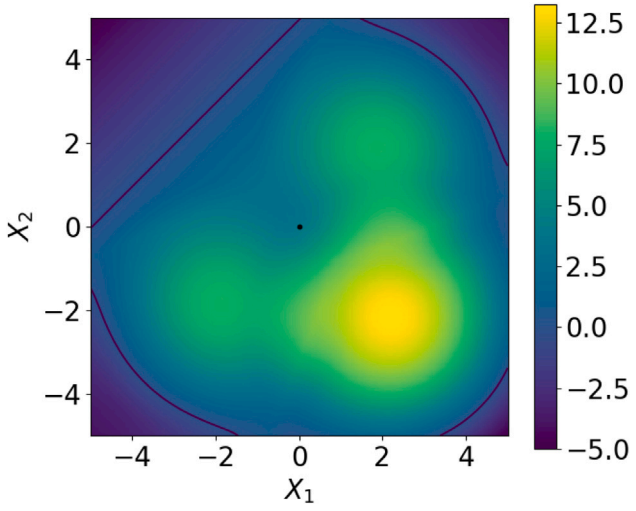

Fig. 8. The modified limit state function $\tilde{g}$ after the additions of Bulge_1, Bulge_2, and Bulge_3.

assumed that $\beta = 5$. The reference probability value computed with the Monte Carlo method is equal to $P_f = 1.15 \times 10^{-6}$ with an empirical CV of 4.1% and a sample of size 5×10^8. There are four failure regions in this failure domain.

The performance of the proposed method was studied in dimensions 200, 300, and 400. As the inputs are standard Gaussian, one has $R^2 \sim \chi^2(d)$. The definition of the important ring is the same as in [30]: the interval [LB, UB] is centered around $\sqrt{d}$ and the smallest value of r such that $\mathbb{P}(\sqrt{d} - r \leq R \leq \sqrt{d} + r) \geq 1 - 10^{-8}$ is selected. The interval becomes $(10.02, 18.26)$ for $d = 200$, $(13.22, 21.42)$ for $d = 300$ and $(15.91, 24.09)$ for $d = 400$. Each of the four failure regions starts before the beginning of the important ring and spreads across it. Thus this application is an example of the situation referred to as Case 2 in the previous sections.

For each of the four failure regions, the converged κ value of the CE-AIS algorithm is the same. This value grows with the dimension. For $d = 200$, the converged κ value is around 79. For $d = 300$, the converged κ value is around 94. Finally for $d = 400$, the converged κ value is around 107. A study of the influence of the initial $\kappa_{i,0}$ in the CE-AIS algorithm of the sampling problem (Section 2.3), simply denoted κ_0, is displayed in Fig. 10.

The number K of failure regions found by the algorithm is displayed in Fig. 10 (c). In dimension 300, where the converged κ value is equal to 94, setting $\kappa_0 = 50$ or $\kappa_0 = 150$ did not prevent the algorithm from finding the four failure regions each time. However, in dimension 200, if κ_0 is greater than the converged value 79, the algorithm finds on rare occasions five failure regions instead of four (once every 500 independent simulations, for $\kappa_0 = 120$ and $\kappa_0 = 150$). This means that the samples generated in one particular failure region were too concentrated and did not cover the whole failure region; as a result, the remaining part was identified as another new failure region (as both the bulge and the cone associated to the representative failing point were not wide enough; see Section 2.4). This is not a problem in terms of failure probability estimation, but it results in a heavier budget N_{samp} for these particular simulation runs.

In contrast in dimension 400, if κ_0 is a lot smaller than the optimal κ equal to 107, the algorithm sometimes failed to find the four failure regions and stopped at three (18 times out of 500 independent simulations, for $\kappa_0 = 50$). Indeed, if κ_0 is too small, then the sample generated in the first step of the CE-AIS algorithm is too wide, and the situation occurs where not a single $R_i \mathbf{T}_i$ is failing. This particular failure region is thus considered as negligible (see Section 2.3) and therefore $K = 3$. The resulting probability estimate is then biased (see Fig. 10 (a)) and the variance of the estimate is higher (see Fig. 10 (d)). However, it should be noted that finding three failure regions or five remained rare instances, and that the algorithm is quite robust regarding the number of failure regions found depending on the value of κ_0.

The fluctuations seen in the probability estimates in Fig. 10 (a) are due to the randomness of the sampling of the CE-AIS algorithm. The probability estimate is very close to the reference value and is not dependent on κ_0, except in dimension 400 when $\kappa_0 = 50$. It seems that the value of κ_0 that minimizes the number N_{samp} of evaluations of the limit state function is when κ_0 is really close to the optimal κ, which is expected (see Fig. 10 (b)). Then, as κ_0 is set greater or smaller, the budget N_{samp} increases as more steps are necessary for the CE-AIS algorithm to converge.

The global numbers $N_{\text{opt},1}$ and $N_{\text{opt},2}$ of evaluations of g and ∇g required for all the optimizations performed in the identification problems did not vary throughout the study. Indeed, as the initial LHS is

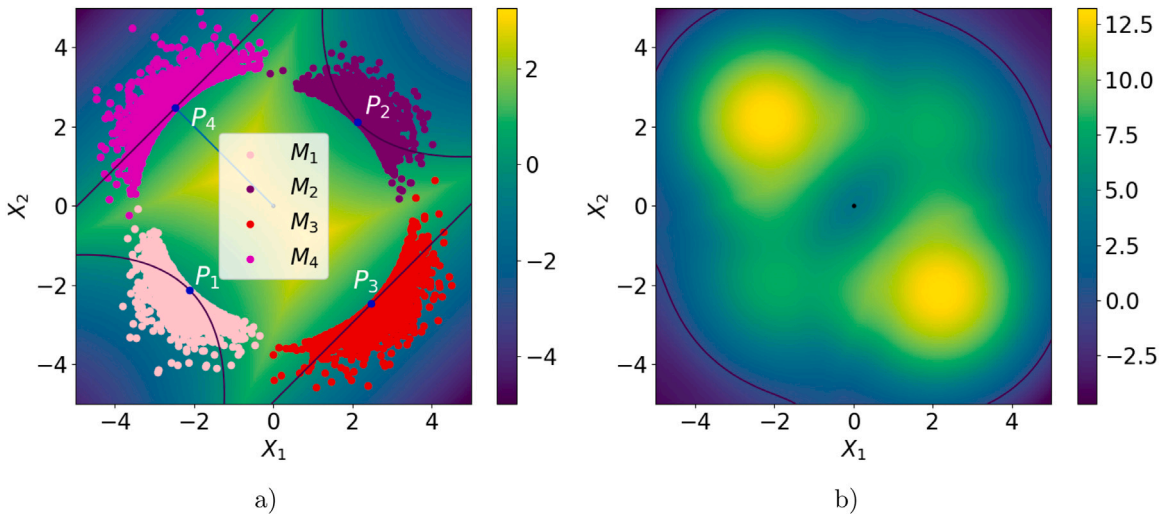

Fig. 9. (a) Sampling of the fourth failure region of the 4-branch system. One has $P_4 = (-2.74, 2.47)$, $r_{\text{opt},4} = 3.49$, and $\nu_4 = (-0.71, 0.71)$. Population M_4 is of size $2N$ as only two iterations were needed in the algorithm, with $\kappa_{4,0} = 20$ and $\kappa_{4,1} = 16.4$. (b) The modified limit state function after the addition of Bulge_4 to the previous modified lsf.

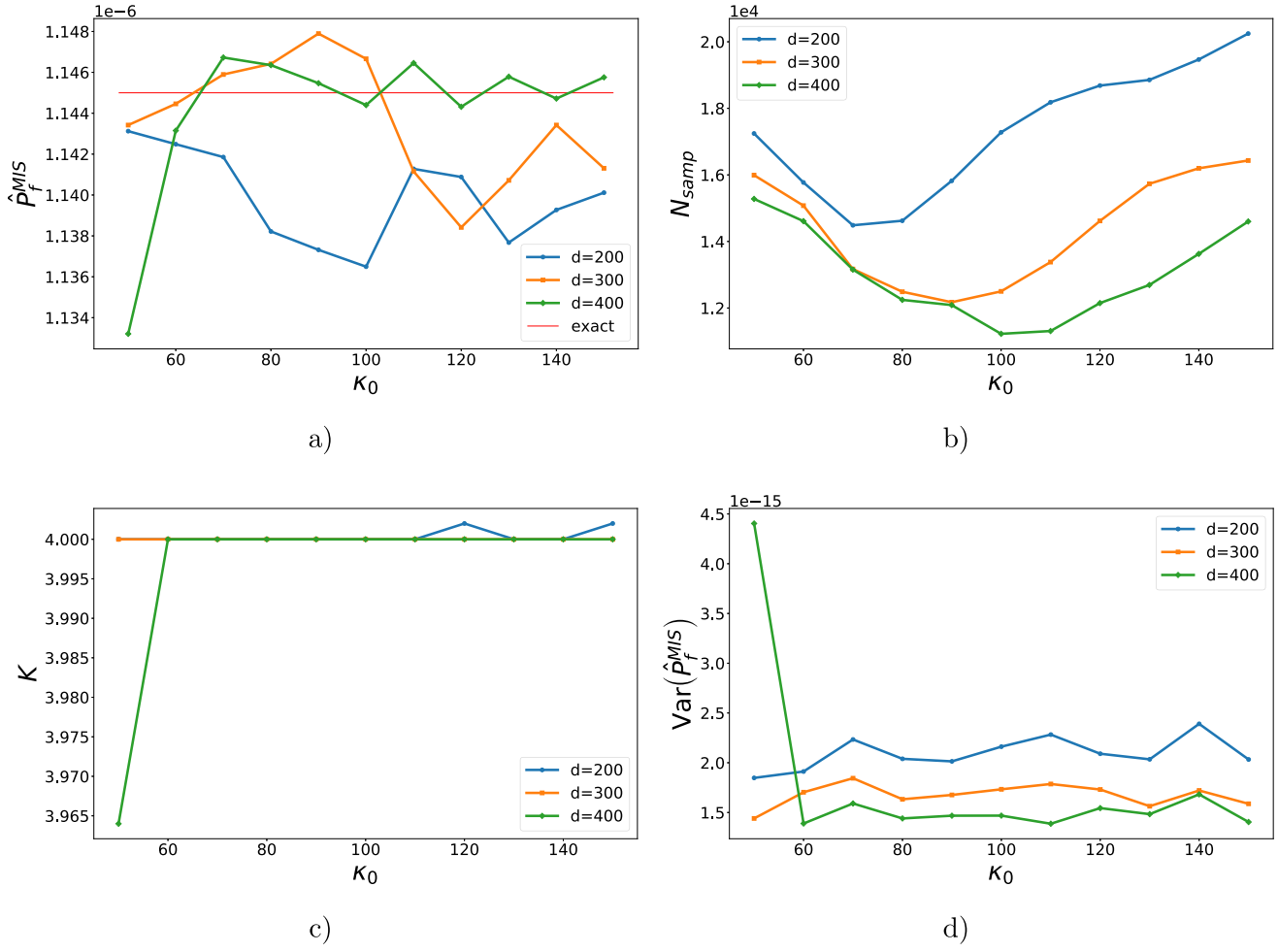

Fig. 10. (a) Evolution of the failure probability estimate with κ_0, for dimensions 200, 300, and 400. (b) Evolution of the number of lsf evaluations N_{samp} with κ_0. (c) Evolution of the number K of failure regions found with κ_0. (d) Evolution of variance of the failure probability estimate with κ_0.

Table 1
Comparison of the proposed algorithm with the iCE-vMFNM algorithm and a SS algorithm for g_1. The reference probability is equal to 1.15×10^{-6} for the three dimensions considered.

Series system of four linear limit state functions						
	Proposed algorithm		iCE-vMFNM		Subset sampling	
$d = 200$						
	1.14×10^{-6}		1.00×10^{-6}		1.15×10^{-6}	
	CV	4.1% (3.9%)	CV	56.4%	CV	10.6%
	N_{samp}	14486	N_{samp}	449400	N_{samp}	91530
	$N_{\text{opt},1}$	261				
	$N_{\text{opt},2}$	204				
$d = 300$						
	1.15×10^{-6}		1.03×10^{-6}		1.15×10^{-6}	
	CV	3.6% (3.6%)	CV	50.6%	CV	10.9%
	N_{samp}	12174	N_{samp}	456800	N_{samp}	91860
	$N_{\text{opt},1}$	231				
	$N_{\text{opt},2}$	184				
$d = 400$						
	1.15×10^{-6}		1.05×10^{-6}		1.15×10^{-6}	
	CV	3.3% (3.4%)	CV	33.1% [**]	CV	10.3%
	N_{samp}	11308	N_{samp}	400000	N_{samp}	91470
	$N_{\text{opt},1}$	255				
	$N_{\text{opt},2}$	213				

of size 10, if the algorithm finds three or five failure regions instead of four, the number of performed optimizations remains the same in the end. Thus κ_0 does not influence the value of these numbers.

The conclusion of this study is to choose κ_0 relatively high when no information concerning the failure regions is available and the higher the dimension, the higher κ_0.

To compare the algorithm with the other available methods, κ_0 was selected as follows: 70 when $d = 200$, 90 when $d = 300$, and 110 when $d = 400$. The performance of the algorithms is summarized in Table 1; the CV displayed for all the methods is the empirical one, estimated over the 500 independent simulation runs. The numbers in parentheses are the mean of the theoretical CV estimates of the proposed method.

The estimates of the proposed method and the subset simulation method are quite close to the reference value, i.e., 1.15×10^{-6}. However, the proposed algorithm has the smallest CV with the smallest global budget. Indeed, the total number $N_{\text{opt},1} + N_{\text{samp}}$ of evaluations of the lsf is very low: with less than 15,000 evaluations, the CV is below 4% whatever the dimension d. For every simulation, the number of failure regions found by the proposed method is equal to 4. The number N_{samp} seems to decrease as the dimension increases; only the scalar parameter κ is optimized with the CE-AIS method. The optimization budgets $N_{\text{opt},1}$ and $N_{\text{opt},2}$ remain negligible compared to the number of lsf evaluations required by the other two methods. The estimates of the theoretical CV are very close to the empirical CV, which suggests that the precision of the algorithm can be correctly determined with only one simulation run.

The iCE-vMFNM algorithm performs poorly compared to the other two algorithms. Indeed, the mean estimate is a bit biased compared to the reference value; the CV is very high and the simulation budget is huge compared to the other two methods. In dimension 400, the displayed statistics result from less than 500 independent simulations, hence the symbol [**], given that the algorithm did not converge most of the time. The $\text{CV}_{\text{target}}$ parameter was set to 10 as it resulted in being the best value after several tests, and the size of the sample per iteration was set quite high for each dimension or else the algorithm would not converge, hence the very large simulation budget. The number $K = 4$ of failure regions is a parameter to be set; therefore, its previous knowledge is required unlike in the proposed algorithm where no assumption is made on K.

The number of evaluations of g_1 for the subset sampling method is independent of the dimension of the inputs. The simulation budget is quite high: at least six times higher than the proposed algorithm global budget. This method leads to large CVs as well: they are two to three times larger than the proposed algorithm estimate CVs.

3.2. Duffing oscillator

The second example is a nonlinear elastic system as described in [39]. The Duffing oscillator is modeled by the equation

$$m\ddot{z}(t) + c\dot{z}(t) + k\{z(t) + \gamma z(t)^3\} = f(t),$$

where $z(t)$, $\dot{z}(t)$, and $\ddot{z}(t)$ are the displacement, velocity, and acceleration of the oscillator at time t, respectively, and the constants are taken as in [39], viz. $m = 1000$ kg, $c = 200\pi$ Ns/m, $k = 1000(2\pi)^2$ N/m and $\gamma = 1$ m^{-2}. The oscillator is subjected to the random loading $f(t, \mathbf{X})$, discretized in the frequency domain as in [33], viz.

$$f(t, \mathbf{X}) = -m\sigma \sum_{i=1}^{d/2} \{X_i \cos(\omega_i t) + X_{d/2+i} \sin(\omega_i t)\},$$

where $\omega_i = i\Delta\omega$ with $\Delta\omega = 30\pi/d$ and $\sigma = \sqrt{2S\Delta\omega}$, where $S = 0.005$ m^2/s^3 is the intensity of the loading. Here, $\mathbf{X}$ is a vector of independent standard Gaussian random variables of dimension d. The lsf g_2 is the maximum displacement of the oscillator at $t = 2$ s defined as

$$g_2(\mathbf{X}) = \min\{z_{\text{crit},1} - z(2s), z(2s) - z_{\text{crit},2}\},$$

where $z_{\text{crit},1} = 0.1$ and $z_{\text{crit},2} = -0.06$. The initial values are set to $z(0) = 0$ and $\dot{z}(0) = 1.5$. The reference value is computed with a Monte Carlo method and is equal to 4.28×10^{-4} with an empirical CV of 4.9% with a sample of size of 10^6, whatever the dimension d. There are two failure regions for this failure domain.

The performance of the proposed method was studied in dimensions 100, 200, and 300 and the important ring was defined as in the previous application. Thus for $d = 100$, the importance interval equals (5.83, 14.17) and for the other two dimensions the interval is the same as in the previous application. Both failure regions start before the beginning of the important ring and spread across it; thus this application is another example of the situation referred to as Case 2 in the previous sections.

To compare the algorithm with the other available methods, the initial values of κ_0 were selected as follows: $\kappa_0 = 50$ when $d = 100$, $\kappa_0 = 70$ when $d = 200$, and $\kappa_0 = 90$ when $d = 300$. These particular values are inspired by the study of the previous example. The

Table 2
Comparison of the proposed algorithm with the iCE-vMFNM algorithm and a SS algorithm for g_2. The reference probability is equal to 4.28×10^{-4} for the three dimensions considered.

Duffing oscillator						
	Proposed algorithm		iCE-vMFNM		Subset sampling	
$d = 100$						
	4.28×10^{-4}		4.28×10^{-4}		4.29×10^{-4}	
	CV	4.7% (4.6%)	CV	5.0%	CV	8.7%
	N_{samp}	5818	N_{samp}	9312	N_{samp}	40000
	$N_{\text{opt},1}$	386				
	$N_{\text{opt},2}$	278				
$d = 200$						
	4.26×10^{-4}		4.26×10^{-4}		4.28×10^{-4}	
	CV	4.0% (4.1%)	CV	5.0%	CV	9.5%
	N_{samp}	5624	N_{samp}	16170	N_{samp}	40000
	$N_{\text{opt},1}$	244				
	$N_{\text{opt},2}$	187				
$d = 300$						
	4.26×10^{-4}		4.25×10^{-4}		4.28×10^{-4}	
	CV	4.5% (4.3%)	CV	4.6%	CV	8.9%
	N_{samp}	5978	N_{samp}	23660	N_{samp}	40000
	$N_{\text{opt},1}$	268				
	$N_{\text{opt},2}$	201				

performance of the algorithms is summarized in Table 2, where the CV displayed for all the methods is the empirical one, estimated over the 500 independent simulation runs. The numbers in parentheses are the mean of the theoretical CV estimates of the proposed method.

The estimates of the three methods are close to the reference value 4.28×10^{-4}. As in the previous example, the proposed algorithm has the smallest CV with the smallest global budget. The total number $N_{\text{opt},1} + N_{\text{samp}}$ of evaluations of the lsf is extremely low: with less than 7000 evaluations, the CV is below 5% whatever the dimension d. For every simulation, the number of failure regions found by the proposed method is equal to 2. Given that the number of failure regions found is twice smaller than in the previous example, it is not surprising that N_{samp} is also twice smaller. It seems that N_{samp} is thus strongly linked to the number of failure regions and completely independent of the dimension. The numbers $N_{\text{opt},1}$ and $N_{\text{opt},2}$ have the same magnitude as in the previous application even though the lsf is more complex; they remain below 400, which is very low compared to N_{samp}. Once again, the estimates of the theoretical CV are very close to the empirical CV.

For this application, the iCE-vMFNM algorithm performs better than in the previous example. The number of lsf evaluations gradually increases, for a CV close to 5%. The size of the sample per iteration is set depending on the dimension d as the model includes a total of $2(d + 3) + (2 - 1)$ parameters that have to be optimized with the improved CE-AIS algorithm [33]. In dimension $d = 300$, the number of lsf evaluations required is still four times higher than with the proposed algorithm. The number of failure regions, $K = 2$, was set as an input of the iCE-vMFNM and for this particular application, the $\text{CV}_{\text{target}}$ parameter was set to 2% as it resulted in being the optimal value after several tests.

The number of evaluations of g_2 for the subset sampling method is the highest with also the highest CV and it is still independent of the dimension. As for the other two methods, this number is lower than in the previous example. The number N_{samp} for the subset sampling method is very high compared to the proposed method, as it is six to seven times superior in size.

3.3. Portfolio loss

The third example is often used in financial studies [40–42]. It consists of a large portfolio of loans with 250 obligors, each of whom having a non-zero probability of default. It is assumed that a $d \times 1$ vector of underlying latent variables $\mathbf{Z}$ represents the obligors as such: when $Z_i > 0.5\sqrt{d}$, then the ith obligor defaults. The portfolio loss is expressed as

$$L(\mathbf{Z}) = \mathbb{I}_{Z_1 > 0.5\sqrt{250}} + \cdots + \mathbb{I}_{Z_{250} > 0.5\sqrt{250}}.$$

The value of interest is the probability that the portfolio loss exceeds 0.25×250; thus, the limit state function is given by

$$g_3(\mathbf{Z}) = 62.5 - L(\mathbf{Z}).$$

This example comprises only one failure region. The inputs $\mathbf{Z}$ are assumed to be centered and their joint distribution is taken to be d-variate Student with $\nu = 4$ degrees of freedom and $d \times d$ dispersion matrix

$$\boldsymbol{D}_{\mathbf{Z}} = \begin{pmatrix} 9 - 8\rho^2 & \rho^2 & . & . & . & \rho^2 \\ \rho^2 & 9 - 8\rho^2 & \rho^2 & . & . & . \\ . & & & & & . \\ . & & & & & . \\ \rho^2 & . & . & . & \rho^2 & 9 - 8\rho^2 \end{pmatrix}$$

with ρ a constant set to 0.25. The reference probability value is equal to 8.12×10^{-3}. To use the proposed method, the first step is to apply a linear transformation to remove the correlation of the inputs. To do so, one has to pre-multiply the inputs $\mathbf{Z}$ by the matrix A^{-1} such that $AA^{\top}$ is the Cholesky decomposition of $\boldsymbol{D}_{\mathbf{Z}}$. The limit state function with the standard variable $\mathbf{X} = A^{-1}\mathbf{Z}$ is then

$$\bar{g}_3(\mathbf{X}) = 62.5 - L(A\mathbf{X}).$$

Given that $\mathbf{X}$ is a standard multivariate Student random vector with $\nu = 4$ degrees of freedom and dimension $d = 250$, then $R^2/250 \sim \mathcal{F}(250, 4)$ with $\mathcal{F}$ a Fisher–Snedecor distribution. This distribution is heavy-tailed and is not symmetric around its mean. The important ring is defined with the two hyperspheres of radius LB and UB based on the quantiles of the Fisher–Snedecor distribution, viz. $q_{10^{-5}/2}(\mathcal{F}(250, 4))$ and $q_{1-10^{-5}/2}(\mathcal{F}(250, 4))$. The important interval is thus equal to $(5.62, 398.22)$ and is a lot wider than for the χ^2 distribution of the previous applications. The failure region then starts inside the important ring; therefore, this application is an example of the situation referred to as Case 1 in the previous sections.

The proposed algorithm requires the gradient of $\bar{g}_3$ for the optimizations performed in the identification problems. Nevertheless, this particular limit state function is not differentiable, as it involves the indicator function in the portfolio loss function L. Thus, only for the optimizations performed in the identification problems, a substitute $\hat{g}_3$

Table 3
Comparison of the proposed algorithm with the VM algorithm of [41] and a classical Monte Carlo for $\bar{g}_3$. The reference probability is equal to 8.12×10^{-3}.

Portfolio Loss							
Proposed algorithm ($N = 1000$)		Proposed algorithm ($N = 13000$)		VM		MC	
8.12×10^{-3}		8.15×10^{-3}		8.14×10^{-3}		8.12×10^{-3}	
CV	8.4% (8.4%)	CV	3.9% (3.7%)	CV	0.5%	CV	1.1%
N_{samp}	7452	N_{samp}	50258	N_{samp}	55000	N_{samp}	10^6
$N_{\text{opt},1}$	1354	$N_{\text{opt},1}$	1340				
$N_{\text{opt},2}$	1119	$N_{\text{opt},2}$	1108				

of $\bar{g}_3$ is used, viz.

$$\hat{g}_3(\mathbf{X}) = 62.5 - \hat{L}(A\mathbf{X}),$$

where

$$\hat{L}(A\mathbf{X}) = \Psi([A\mathbf{X}]_1 - 0.5\sqrt{250}) + \cdots + \Psi([A\mathbf{X}]_{250} - 0.5\sqrt{250})$$

with Ψ being the cdf of the standard Gaussian law. This regularization for the indicator function is quite common (as derived in [46]) and makes differentiation possible.

The performance of the proposed algorithm is displayed in Table 3 with $\kappa_0 = 80$ for $N = 1000$ and $N = 13{,}000$. The numbers in parentheses are the theoretical coefficients of variation of the proposed method. The results are compared with a variance minimization algorithm (VM) from [41] and a classical Monte Carlo algorithm. The iCE-vMFNM algorithm and the SS algorithm were not used for this application as the inputs are not normally distributed.

For every simulation, the number of failure region found by the proposed method is equal to 1. Compared to the two previous examples, the proposed algorithm here is not as precise in terms of CV. Indeed, a very large budget is needed to reach a CV value lower than 4%, even though there is only one failure region. Since the important interval is wide for this particular elliptical law, the conditional distribution selected as an IS density for the radial component R may not be the most appropriate parametric distribution. Also, as there is only one failure region here, the proposed algorithm is probably not best suited.

The VM algorithm, in contrast, is very precise. However, to achieve such results, it is assumed that it is possible to generate observations from h_{opt}, the optimal IS density in Eq. (3), with a Markov Chain Monte Carlo (MCMC) algorithm. This assumption is reasonable in this particular case as there is only one failure region. The VM algorithm would take a very long time to converge if there were several failure regions and is not applicable on the first two examples considered in this paper.

In the end, the proposed algorithm remains relevant, as it makes it possible to compute the probability with a CV lower than 10% with a budget lower than 10,000. Furthermore, the estimates of the theoretical CV are still very close to the empirical CV. This example with the Student distribution shows the flexibility of the proposed algorithm in terms of elliptically distributed inputs.

3.4. Airfoil in inviscid transonic flow

3.4.1. Description of the problem and optimal airfoil

The last example is inspired by an optimization test case provided by the Computational Fluid Dynamic (CFD) solver SU2 [43]. For the sake of completeness, the main features of this problem are now detailed. The objective of this test case is to design the shape of an airfoil that minimizes the drag coefficient in transonic inviscid flow conditions. The baseline shape is a NACA 0012 airfoil, the freestream pressure is set to 101,325 Pa, its temperature is set to 273.15 K and the Mach number is equal to 0.8. The 2D Euler fluid model is solved by the finite-volume method on a computational mesh of 5233 points and 10,216 triangular elements. Fig. 11 (a) presents the mesh around the airfoil. Under such conditions, a transonic shock appears on the upper surface of the airfoil leading to a high drag coefficient equal to $C_D^{\text{NACA }0012} = 2.13 \times 10^{-2}$, as presented in Fig. 11 (b).

The shape of the airfoil is parameterized through Hicks–Henne bump functions defined around the airfoil. These functions include two parameters, the location of their center and the amplitude of the bump. For this example, 10 Hicks–Henne bump functions are used, five on the upper surface of the airfoil and five on the lower surface of the airfoil, respectively centered at 5%, 25%, 50%, 75%, 95% of the airfoil chord. The optimization problem is then to minimize the drag coefficient with respect to the 10 amplitudes of the Hicks–Henne bump functions, under a constraint of lift coefficient equals to $C_L = 0.326$ (value obtained with the initial NACA 0012 airfoil). This problem is solved using a gradient-based optimizer and the gradient of the objective function is obtained through an adjoint approach. Readers interested in the details of this resolution are referred to the SU2 tutorials and to the many articles about the adjoint approach in CFD computation; see [47] for example.

The solution of the optimization problem is illustrated in Fig. 12. One can note that the optimal solution (Fig. 12 (a)) reaches some characteristics of a supercritical airfoil, as a flattened upper surface near the leading edge. The obtained pressure coefficient field (Fig. 12 (b)) shows no transonic shock and leads to an overall drag coefficient equal to $C_D^{\text{opt}} = 1.02 \times 10^{-3}$.

3.4.2. Reliability problem

It is now assumed that the optimal airfoil shape previously defined is subjected to random distortion. This distortion is represented by 100 Hicks–Henne bump functions, 50 at the lower airfoil surface and 50 at the upper airfoil surface. The centers of the 50 functions are linearly spaced between 5% and 95% of the airfoil chord. It is assumed that the amplitudes of the Hicks–Henne functions are independent and normally distributed. The mean value is null and the variance is chosen to create reasonable deformations of the airfoil, modeling manufacturing uncertainties for example. With previous notations, this leads to $\mathbf{X} \sim \mathcal{N}(\mathbf{0}, 2.5 \times 10^{-7} \times \mathbf{I}_d)$. A failure of the system occurs when the distortion causes a value of the drag coefficient that is above a certain threshold equal to 0.01; thus the limit state function is written

$$g_4(\mathbf{X}) = 0.01 - C_D(\mathbf{X}).$$

First a Monte Carlo estimation is performed in order to get a reference value for this problem. A total of 106,770 simulations were run leading to a failure probability estimation equal to $P_f^{\text{MC}} = 5.61 \times 10^{-4}$ with a theoretical coefficient of variation of 12.9%. Each CFD simulation was run on a cluster using 24 CPU and took approximately $7s$. The Monte Carlo estimation thus lasted approximately 8.5 days on 24 CPU.

The approach proposed in this article is now applied to this example. The definition of the important ring is the same as in Section 3.2, but given that the standard deviation of the inputs is equal to 5×10^{-4}, the bounds of the importance interval are multiplied by 5×10^{-4} as well, and $\text{IR} = (2.92 \times 10^{-3}, 7.08 \times 10^{-3})$. The equations between the inputs $\mathbf{X}$ and the resulting drag coefficient C_D are the Euler and adjoint Euler

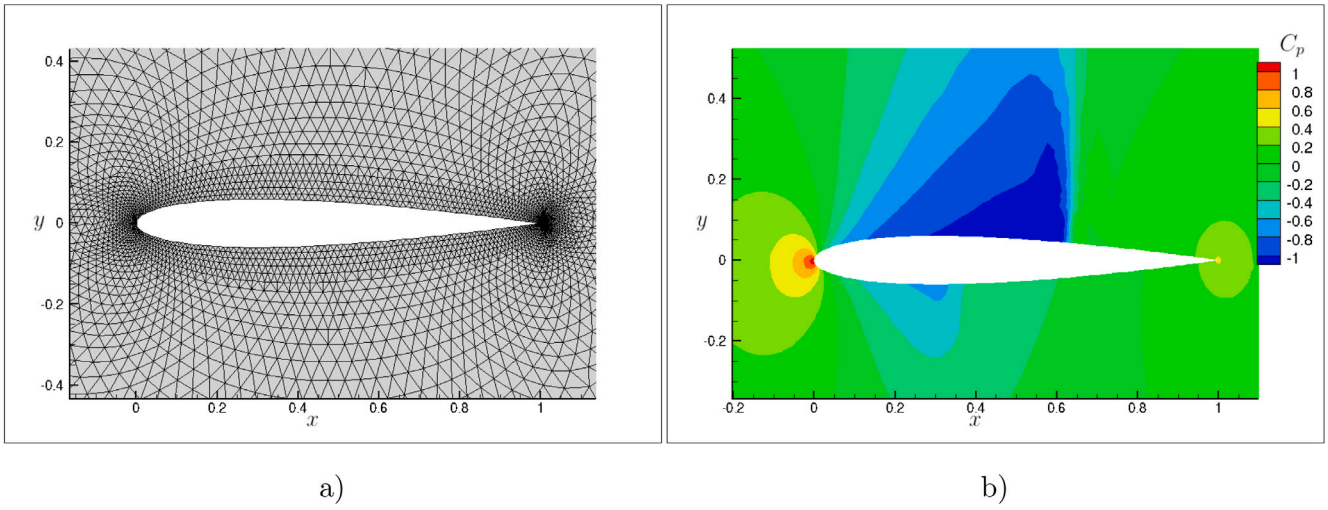

Fig. 11. (a) Close view on the initial computational mesh of the NACA 0012 airfoil. (b) Pressure coefficient field showing the transonic shock on the NACA 0012 airfoil.

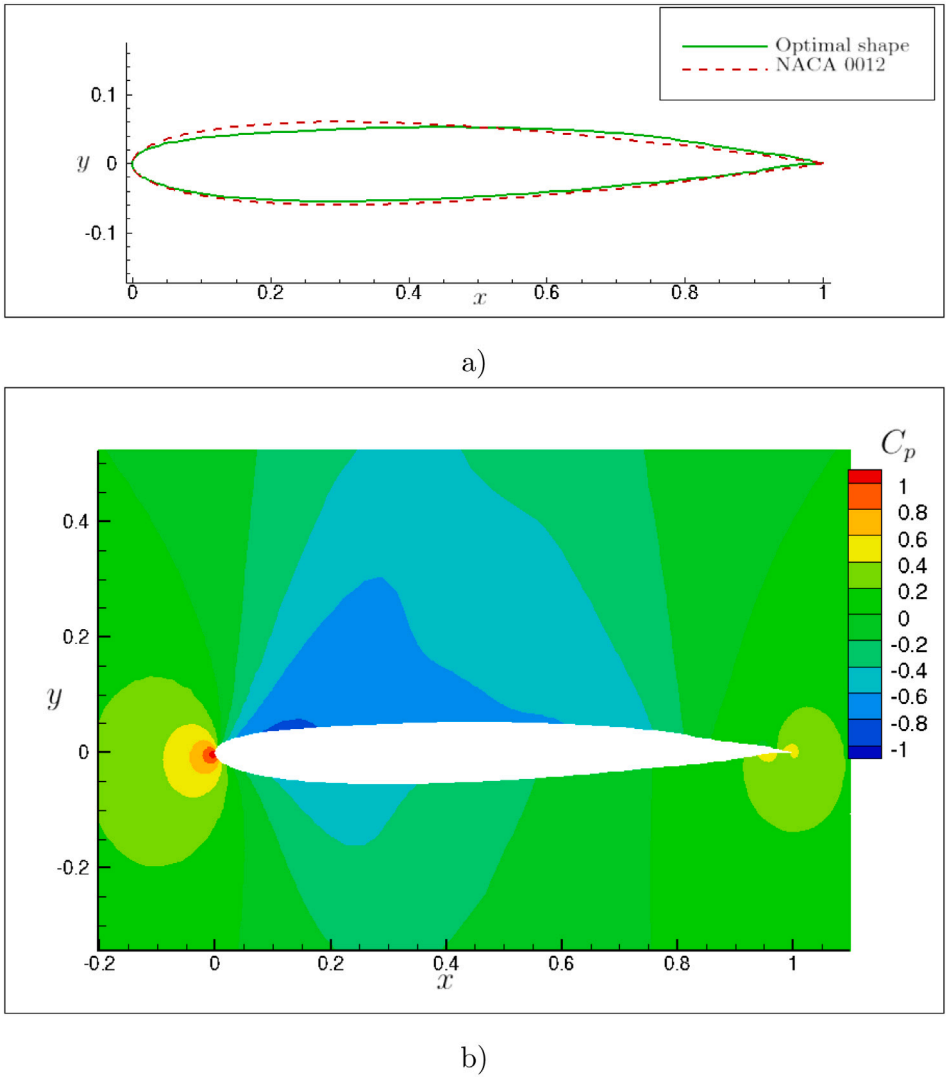

Fig. 12. (a) Comparison between the optimal airfoil solution and the baseline NACA 0012 airfoil. (b) Pressure coefficient field around the optimal solution.

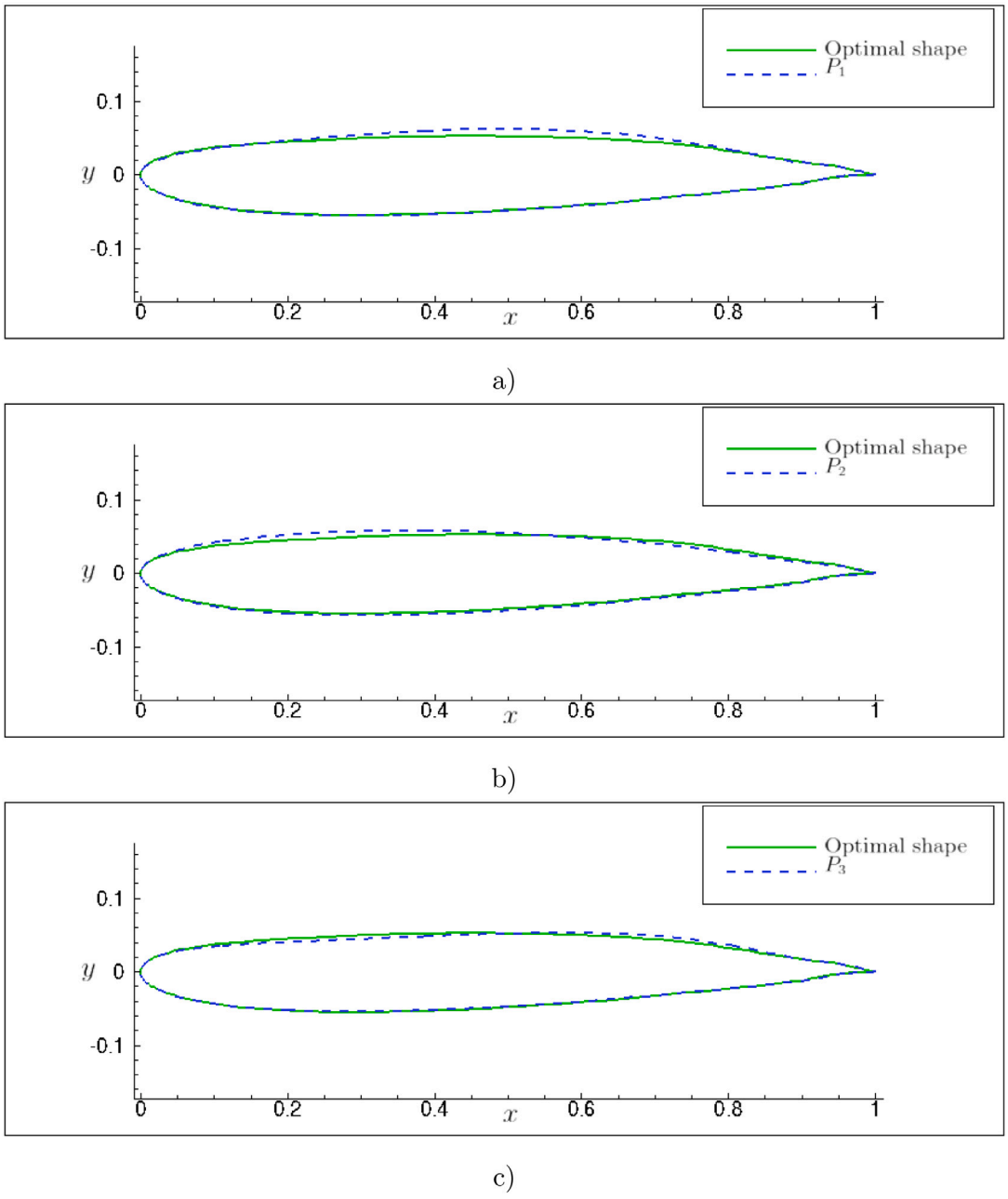

Fig. 13. Shape comparison between the optimal airfoil and the critical point found by the proposed approach: (a) P_1, (b) P_2, (c) P_3.

equations. The lsf for this engineering problem is a black-box function as the analytical form of the drag coefficient C_D is not available but numerically computed by the finite-volume CFD code. One can note that it is thus impossible to know *a priori* the number of failure regions.

The proposed algorithm found $K = 3$ different failure regions. For each failure region, the representative point P_i was found on the lower bound LB of the important ring. The vector values of these three points represent the worst configurations for the shape of the airfoil. Indeed they lead to shapes that produce particularly high drag. The shapes induced by the three representative failing points P_1, P_2 and P_3 are displayed in Fig. 13. The pressure fields resulting from these three shapes are illustrated in Fig. 14. Shocks appear which explain the high drag of these shapes. Indeed, for the point P_1 a large deformation appears at the rear of the airfoil causing a strong acceleration of the flow on this part and thus a transonic shock on the rear of the airfoil; see Fig. 14 (a). The point P_2 deforms the optimal shape near the leading edge and curves the airfoil in this area. The P_2 deformed shape looks approximately like the original NACA 0012 airfoil and thus leads to a transonic shock; see Fig. 14 (b). The point P_3 results from a negative curvature at the leading edge side and a bump at the trailing edge side. This deformation creates two transonic shocks as shown in Fig. 14 (c).

Table 4
Comparison of the proposed algorithm with the Monte Carlo method for g_4.

Failure probability of the airfoil shape			
Proposed algorithm		Monte Carlo	
5.30×10^{-4}		5.61×10^{-4}	
CV	9.8%	CV	12.9%
N_{samp}	13000	N_{samp}	106770
$N_{\text{opt},1}$	4717		
$N_{\text{opt},2}$	918		

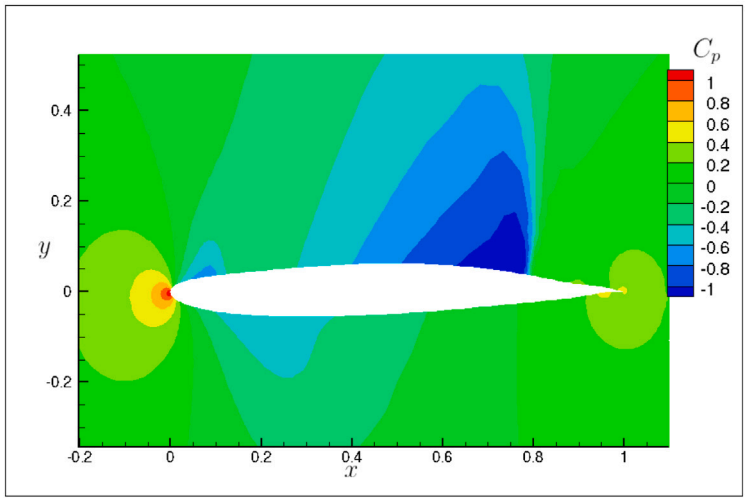

a)

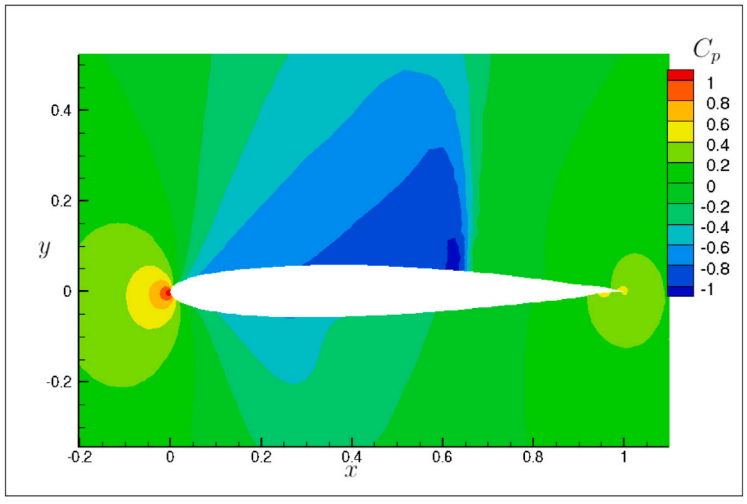

b)

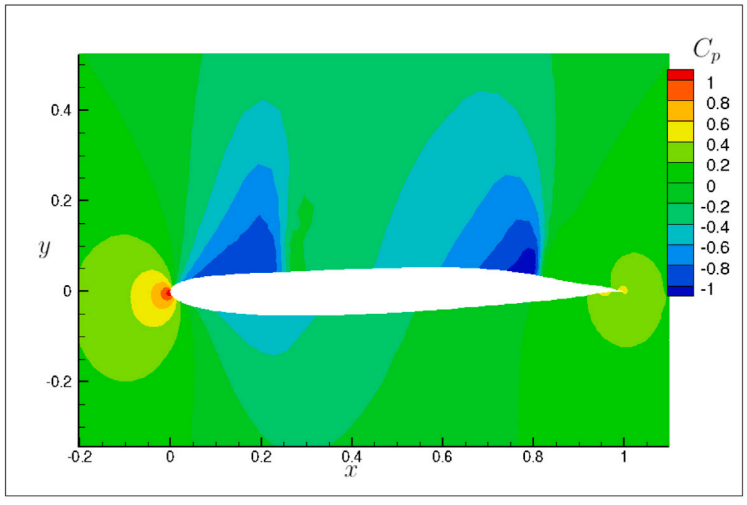

c)

Fig. 14. Pressure coefficient fields at the critical point found by the proposed approach: (a) P_1, (b) P_2, (c) P_3.

The performance of the proposed algorithm is summarized in Table 4, where the coefficients of variation are the theoretical ones. One can note that the failure probability found by the proposed algorithm is very close to the Monte Carlo reference, and has a smaller coefficient of variation. Compared to the Monte Carlo estimation, the simulation budget is divided by a factor close to 7, which is a very interesting gain for such a costly numerical application. This example also shows the value of finding the important failure regions in the input space as this information can further help to understand the critical failure mechanisms and help the design. It should be noted that the proposed algorithm was run two more times, and on both occasions the same three different failure regions were found (with small differences due to numerical precision).

4. Conclusions

This paper presents a new algorithm that estimates the failure probability of a high-dimensional system whose failure domain encompasses several failure regions. It follows the work of [32,33] as it takes advantage of the stochastic decomposition of the elliptical inputs to create flexible IS densities for each of the failure regions. The search for the failure regions is inspired by the FORM method [8] but innovative as the important ring is taken into account in the optimization problems performed in the standard elliptical input space. The parameters of the proposed IS densities are set thanks to the performed optimizations and the cross-entropy method. A mixture of the IS auxiliary densities is gradually constructed and the failure probability is then computed with a MIS estimate.

The performance of this algorithm is demonstrated with four numerical examples: three with the Gaussian distribution and one with the Student distribution. The results underline the great efficiency of the proposed method, as the number of lsf evaluations is consistently lower than the one obtained with other methods, with a comparable accuracy with respect to the bias and variance. The algorithm is simple to parameterize, as only κ_0 and N have to be set.

In this paper, it was assumed that the gradient of the limit state function is available for the optimization problems in the elliptical input space. When the gradient is unavailable, these optimizations are very difficult to perform in high-dimensional space and the proposed algorithm may be inefficient. However, new methods recently presented in [48,49] make it possible to find the design points for the FORM in high-dimensional standard normal space without resorting to the gradient. Combining these new optimization schemes with the proposed algorithm could be a promising alternative to the requirement that the gradient is known.

CRediT authorship contribution statement

Marie Chiron: Writing – original draft, Visualization, Software, Methodology, Investigation, Formal analysis, Conceptualization. **Christian Genest:** Writing – review & editing, Validation, Supervision, Methodology, Conceptualization. **Jérôme Morio:** Writing – review & editing, Validation, Supervision, Methodology, Investigation, Conceptualization. **Sylvain Dubreuil:** Writing – review & editing, Validation, Supervision, Methodology, Conceptualization.

Declaration of competing interest

The authors declare that they have no known competing financial interests or personal relationships that could have appeared to influence the work reported in this paper.

Data availability

No data was used for the research described in the article.

Acknowledgments

The first author was supported by the MINT research school (Future Investments Program (PIA) of the French National Research Agency (ANR), Grant No. ANR-18-EURE-0023) and by ISAE-Supaero during her stay at McGill University (Montréal, Canada) as a visiting researcher. This funding is gratefully acknowledged. The second author acknowledges continuing financial support from the Canada Research Chairs Program, the Natural Sciences and Engineering Research Council of Canada, and the Trottier Institute for Science and Public Policy.

References

[1] Genest C, Favre A-C, Béliveau J, Jacques C. Metaelliptical copulas and their use in frequency analysis of multivariate hydrological data. Water Resour Res 2007;43(9).
[2] Genest C, Nešlehová J. Copulas and copula models. second ed.. Encycl Environmetrics 2012;2:541–53.
[3] Fang K-T, Kotz S, Ng KW. Symmetric multivariate and related distributions. Chapman & Hall/CRC; 2018.
[4] Ditlevsen O, Madsen HO. Structural reliability methods. vol. 178, Wiley New York; 1996.
[5] Schueller GI, Pradlwarter HJ, Koutsourelakis P-S. A critical appraisal of reliability estimation procedures for high dimensions. Probab Eng Mech 2004;19(4):463–74.
[6] Zhang J, Xiao M, Gao L, Chu S. A combined projection-outline-based active learning Kriging and adaptive importance sampling method for hybrid reliability analysis with small failure probabilities. Comput Methods Appl Mech Engrg 2019;344:13–33.
[7] Tabandeh A, Jia G, Gardoni P. A review and assessment of importance sampling methods for reliability analysis. Struct Saf 2022;97:102216.
[8] Der Kiureghian A, Dakessian T. Multiple design points in first and second-order reliability. Struct Saf 1998;20(1):37–49.
[9] Echard B, Gayton N, Lemaire M. AK-MCS: An active learning reliability method combining Kriging and Monte Carlo simulation. Struct Saf 2011;33(2):145–54.
[10] Xiao S, Oladyshkin S, Nowak W. Reliability analysis with stratified importance sampling based on adaptive Kriging. Reliab Eng Syst Saf 2020;197:106852.
[11] Menz M, Dubreuil S, Morio J, Gogu C, Bartoli N, Chiron M. Variance based sensitivity analysis for Monte Carlo and importance sampling reliability assessment with Gaussian processes. Struct Saf 2021;93:102116.
[12] Jiang Z-m, Feng D-C, Zhou H, Tao W-F. A recursive dimension-reduction method for high-dimensional reliability analysis with rare failure event. Reliab Eng Syst Saf 2021;213:107710.
[13] Zuniga MM, Murangira A, Perdrizet T. Structural reliability assessment through surrogate based importance sampling with dimension reduction. Reliab Eng Syst Saf 2021;207:107289.
[14] Morio J, Balesdent M, Jacquemart D, Vergé C. A survey of rare event simulation methods for static input–output models. Simul Model Pract Theory 2014;49:287–304.
[15] Au S-K, Beck JL. Estimation of small failure probabilities in high dimensions by subset simulation. Probab Eng Mech 2001;16(4):263–77.
[16] Katafygiotis LS, Cheung S. Application of spherical subset simulation method and auxiliary domain method on a benchmark reliability study. Struct Saf 2007;29(3):194–207.
[17] Au S-K, Beck JL. Important sampling in high dimensions. Struct Saf 2003;25(2):139–63.
[18] Owen AB. Monte Carlo theory, methods and examples. 2013.
[19] Koutsourelakis P-S, Pradlwarter HJ, Schueller GI. Reliability of structures in high dimensions, part I: algorithms and applications. Probab Eng Mech 2004;19(4):409–17.
[20] Papaioannou I, Straub D. Combination line sampling for structural reliability analysis. Struct Saf 2021;88:102025.
[21] Ditlevsen O, Melchers RE, Gluver H. General multi-dimensional probability integration by directional simulation. Comput Struct 1990;36(2):355–68.
[22] Cheng K, Papaioannou I, Lu Z, Zhang X, Wang Y. Rare event estimation with sequential directional importance sampling. Struct Saf 2023;100:102291.
[23] Harbitz A. An efficient sampling method for probability of failure calculation. Struct Saf 1986;3(2):109–15.
[24] Grooteman F. Adaptive radial-based importance sampling method for structural reliability. Struct Saf 2008;30(6):533–42.
[25] Thedy J, Liao K-W. Multisphere-based importance sampling for structural reliability. Struct Saf 2021;91:102099.
[26] Zhang X, Lu Z, Cheng K. Cross-entropy-based directional importance sampling with von Mises–Fisher mixture model for reliability analysis. Reliab Eng Syst Saf 2022;220:108306.
[27] Banerjee A, Dhillon IS, Ghosh J, Sra S, Ridgeway G. Clustering on the unit hypersphere using von Mises–Fisher distributions. J Mach Learn Res 2005;6(9).
[28] Ester M, Kriegel H-P, Sander J, Xu X. A density-based algorithm for discovering clusters in large spatial databases with noise. In: Kdd. 96, (34):1996, p. 226–31.

[29] Klawonn F, Höppner F, Jayaram B. What are clusters in high dimensions and are they difficult to find? In: International Workshop on Clustering High-DImensional Data. Springer; 2012, p. 14–33.
[30] Katafygiotis LS, Zuev KM. Geometric insight into the challenges of solving high-dimensional reliability problems. Probab Eng Mech 2008;23(2–3):208–18.
[31] Leng Y, Lu Z-H, Cai C-H, Li C-Q, Zhao Y-G. Ring simulation: A novel simple and efficient simulation method for structural reliability analysis. Struct Saf 2022;96:102182.
[32] Wang Z, Song J. Cross-entropy-based adaptive importance sampling using von Mises–Fisher mixture for high dimensional reliability analysis. Struct Saf 2016;59:42–52.
[33] Papaioannou I, Geyer S, Straub D. Improved cross entropy-based importance sampling with a flexible mixture model. Reliab Eng Syst Saf 2019;191:106564.
[34] Uribe F, Papaioannou I, Marzouk YM, Straub D. Cross-entropy-based importance sampling with failure-informed dimension reduction for rare event simulation. SIAM/ASA J Uncertain Quantif 2021;9(2):818–47.
[35] Rubinstein RY, Kroese DP. The cross-entropy method: A unified approach to combinatorial optimization, Monte Carlo Simulation, and Machine Learning. vol. 133, Springer; 2004.
[36] Kurtz N, Song J. Cross-entropy-based adaptive importance sampling using Gaussian mixture. Struct Saf 2013;42:35–44.
[37] Lebrun R, Dutfoy A. A generalization of the nataf transformation to distributions with elliptical copula. Probab Eng Mech 2009;24(2):172–8.
[38] Jia G, Tabandeh A, Gardoni P. A density extrapolation approach to estimate failure probabilities. Struct Saf 2021;93:102128.
[39] Zuev K. Advanced stochastic simulation methods for solving high-dimensional reliability problems. Hong Kong University of Science and Technology (Hong Kong); 2009.
[40] Bassamboo A, Juneja S, Zeevi A. Portfolio credit risk with extremal dependence: Asymptotic analysis and efficient simulation. Oper Res 2008;56(3):593–606.
[41] Chan JC, Kroese DP. Improved cross-entropy method for estimation. Stat Comput 2012;22(5):1031–40.
[42] El Masri M, Morio J, Simatos F. Improvement of the cross-entropy method in high dimension for failure probability estimation through a one-dimensional projection without gradient estimation. Reliab Eng Syst Saf 2021;216:107991.
[43] Economon TD, Palacios F, Copeland SR, Lukaczyk TW, Alonso JJ. SU2: An open-source suite for multiphysics simulation and design. AIAA J 2016;54(3):828–46. http://dx.doi.org/10.2514/1.J053813, arXiv:https://doi.org/10.2514/1.J053813.
[44] Sahin FE. Open-source optimization algorithms for optical design. Optik 2019;178:1016–22.
[45] Shields MD, Teferra K, Hapij A, Daddazio RP. Refined stratified sampling for efficient Monte Carlo based uncertainty quantification. Reliab Eng Syst Saf 2015;142:310–25.
[46] Lacaze S, Brevault L, Missoum S, Balesdent M. Probability of failure sensitivity with respect to decision variables. Struct Multidiscip Optim 2015;52(2):375–81.
[47] Kenway GK, Mader CA, He P, Martins JR. Effective adjoint approaches for computational fluid dynamics. Prog Aerosp Sci 2019;110:100542.
[48] Zhong C, Wang M, Dang C, Ke W, Guo S. First-order reliability method based on Harris–Hawks optimization for high-dimensional reliability analysis. Struct Multidiscip Optim 2020;62(4):1951–68.
[49] Zhu S-P, Keshtegar B, Seghier MEAB, Zio E, Taylan O. Hybrid and enhanced PSO: Novel first order reliability method-based hybrid intelligent approaches. Comput Methods Appl Mech Engrg 2022;393:114730.